

The magnetic field and in-situ stress dependence of elastic behavior in EuTiO_3 from resonant ultrasound spectroscopy

Jason Schiemer,¹ Leszek J. Spalek,^{2,3} Siddharth S. Saxena,² Christos Panagopoulos,^{4,5} Takuro Katsufuji,⁶ Annette Bussmann-Holder,⁷ Jürgen Köhler,⁷ and Michael A. Carpenter^{1,*}

¹*Department of Earth Sciences, University of Cambridge, Downing Street, Cambridge CB2 3EQ, UK*

²*Cavendish Laboratory, University of Cambridge, Madingley Road, Cambridge CB3 0HE, UK*

³*Institute of Physics, Cracow University of Technology, Podchorążych 1, 30-084 Krakow, Poland*

⁴*Division of Physics and Applied Physics, Nanyang Technological University, 637371 Singapore, Singapore*

⁵*Department of Physics, University of Crete and FORTH, GR- 71003 Heraklion, Greece*

⁶*Department of Physics, Waseda University, Tokyo 169-8555, Japan*

⁷*Max-Planck Institute for Solid State Research, Heisenbergstrasse 1, Stuttgart D-70569, Germany*

(Dated: December 16, 2015)

Magneto-electric coupling phenomena in EuTiO_3 are of considerable fundamental interest and are also understood to be key to reported multiferroic behavior in strained films, which exhibit distinctly different properties to the bulk. Here the magneto-elastic coupling of EuTiO_3 is investigated by resonant ultrasound spectroscopy with in-situ applied magnetic field and stress as a function of temperature ranging from temperatures above the structural transition temperature, T_S , to below the antiferromagnetic ordering temperature T_N . One single crystal and two polycrystalline samples are investigated and compared to each other. Both paramagnetic and diamagnetic transducer carriers are used, allowing an examination of the effect of both stress and magnetic field on the behaviour of the sample. The properties are reported in constant field/variable temperature and in constant temperature/variable field mode where substantial differences between both data sets are observed. In addition, elastic and magnetic poling at high fields and stresses at low temperature has been performed in order to trace the history dependence of the elastic constants. Four different temperature regions are identified, characterized by unusual elastic responses. The low temperature phase diagram has been explored and found to exhibit rich complexity. The data evidence a considerable relaxation of elastic constants at high temperatures, but with little effect from magnetic field alone above 20 K, in addition to the known low temperature coupling.

PACS numbers: 75.80.+q, 75.85.+t, 62.40.+i

I. INTRODUCTION

EuTiO_3 (ETO) has recently been the subject of a considerable surge in interest owing to its unusual magneto-electrical (ME) coupling behavior, which has its origins in the combination of incipient ferroelectric ordering together with antiferromagnetic (AFM) ordering below $\sim 5.5 \text{ K}$ ¹⁻¹⁸. This makes ETO a magnetically ordered analogue to the intensively studied material SrTiO_3 (STO). Significant interaction exists between the spin ordering and the soft polar phonon mode, since the expected increase and subsequent saturation of the dielectric constant at low temperature is disrupted at the Néel temperature¹⁹, where a drop in the dielectric constant is observed due to stiffening of the soft mode. This effect can be suppressed by application of magnetic fields below T_N , inducing a recovery in the dielectric constant of up to 7 %² which corresponds to a huge magneto-electrical coupling effect.

The existence of multiferroicity is rare, as it has been conventionally understood that an empty d band on the B site ion is required for PbTiO_3 -like “Slater” mode ferroelectricity (induced by the second order Jahn-Teller, SOJT, effect). However, often the only possible source of magnetism is a transition metal ion on the B site, which obviously requires unpaired electrons. This con-

flict is overcome in ETO by having unpaired and highly localised $\text{Eu } 4f^7$ spins at the A site, with $\text{Ti } (d^0)$ on the B site. Nonetheless, ETO is not a true multiferroic, since it does not display both ferroelectricity and ferromagnetism in the absence of applied field, and the segregation of orbital behaviours is not complete, as there are significant interactions between the two sites.

The strong magneto-electric (ME) coupling effect has increased interest in ETO and various theoretical and experimental approaches have been used to examine it. From DFT²⁰, using GGA+U calculations, it was concluded that the hybridization of Eu f orbitals with Ti d orbitals has a significant impact on magnetism and suppresses the second order Jahn-Teller (SOJT) effect that leads to ferroelectricity in other perovskite titanates. The polar soft mode does not extrapolate to zero frequency above zero temperature, even before quantum fluctuations, and therefore ETO is not a true quantum paraelectric (unlike nonmagnetic SrTiO_3 ²¹). The result, that orbital hybridization through Ti d orbitals is key to the exchange pathway, is analogous to that found by Akamatsu *et al.*²² who use DFT with Hartree-Fock hybrid functionals instead of GGA+U. Similarly, Ryan *et al.*²³ describe the mechanism of antiferromagnetism as being related to a 3rd nearest neighbor (NN) superexchange between Eu atoms via both Ti d orbitals and Eu 5d orbitals, using a combination of calculations and XRRMS

experiments.

The nature of the coupling of the magnetic order to an applied electric field has also been investigated. Birol and Fennie²⁰ show that forcing ferromagnetic alignment with high applied field leads to a reinstatement of the SOJT distortion and greater local electrical polarization. Conversely, Ryan *et al.* demonstrate that the 3rd NN superexchange can be significantly altered by the application of an electric field, as the field displaces Ti atoms and changes the overlap angles between the relevant orbitals, leading to a suppression of the AFM order globally and an increase in FM order locally. Glinchuk *et al.*²⁴, using Landau-Ginzburg-Devonshire theory, predict that a high enough electric field will induce a ferromagnetic state, even in the absence of applied strain. Experimentally, work by Li *et al.* on $\text{Eu}_{0.5}\text{Ba}_{0.5}\text{TiO}_3$ films²⁵ shows that the formation of Ti^{III} , induced in this case by oxygen vacancies, can yield ferromagnetism at low T through coupling between Eu^{II} ions, supporting the above conclusions with respect to Ti orbital involvement.

The role of strain both on the ME coupling and in the separate couplings of strain with magnetism and with electrical order has been examined by only a few authors. Interest in this aspect of ETO has been significantly increased by the theoretical prediction^{26,27} that strain engineering can drive ETO into ferromagnetic order with a large ferroelectric polarization. This prediction was subsequently confirmed²⁸ in thin films grown epitaxially on DyScO_3 substrates. Morozovska *et al.*²⁹ predict that it should be possible to create both ferroelectricity and ferromagnetism in ETO nanowires due to surface stresses and the magneto-electro-elastic coupling. It seems, however, that the actual behavior of strained ETO may be less straightforward in real systems than suggested. For instance, Geng *et al.*³⁰ showed, using magnetic force microscopy, that epitaxially strained ETO can have an inhomogeneous magnetic state with both ferromagnetic and nonferromagnetic regions.

An additional level of complexity in ETO beyond the ME coupling below T_N is apparently the interplay between an oxygen rotational instability and electrical and magnetic ordering. While the structure of ETO was originally believed to remain cubic at all temperatures, both theoretical predictions and a number of investigations have subsequently shown a $\text{Pm}\bar{3}\text{m}$ to I4/mcm , cubic to tetragonal (C-T) phase transition. Rushchanskii *et al.*³¹ showed from first principles that a number of antiferrodistorted structures are both extremely close in energy to one another and lower in energy than the prototypical cubic perovskite structure. They also found a spin-phonon coupling, with induced ferromagnetism hardening the octahedral tilting phonon mode significantly, 50 cm^{-1} , in I4/mcm due to the relationship to Eu-Eu angles, but softening slightly, 17 cm^{-1} , in $\text{R}\bar{3}\text{c}$. The tilting transition was first discovered experimentally in specific heat measurements at 282 K by Bussmann-Holder *et al.*⁵ and subsequently by Petrovic *et al.*¹¹, at 283 K and Spalek¹⁸ at 284 K. This is a structural phase transition involv-

ing antiphase octahedral tilting about one of the cubic perovskite axes, with an R point soft mode⁷. Caslin *et al.*¹⁴ conclude from experimental and theoretical results that the spin-phonon coupling remains active far above T_N , with breaks in slope in their χT data, where χ is the magnetic susceptibility, at the C-T tilting transition (282 K) and separately at ~ 75 K.

The precise nature and temperature of this transformation remain contentious, with reports of the transition occurring somewhere between 300 K and 100 K, with variability found between both samples and measurement techniques, and with some mentioning incommensurate behavior. Goian *et al.*'s samples⁹ showed incommensurate reflections in electron diffraction at room temperature after heating from 100 K, but these disappeared after a few days. Kim *et al.*¹² also observed incommensurate octahedral tilt (OT) ordering with disappearance of the reflections two weeks after the samples were prepared. Their modulated structure disappeared completely at temperatures higher than 285 K, and simple tilt reflections were found in addition to the incommensurate reflections from 2 K to 160 K. Diffuse scattering was also present and was attributed to local antiferroelectric displacements of Ti with accompanying local changes in octahedral rotation angle. There also appear to be significant differences between polycrystalline and single crystal samples of ETO. For example, Goian *et al.*⁹ examined standard and high pressure synthesised ETO ceramics, and single crystals. Using diffraction techniques and infrared spectroscopy they observed a transition at ~ 300 K in the conventional ceramic, but no transition down to ~ 100 K in single crystals.

There is some debate in the literature regarding the structure of ETO below T_S . For example, Ellis *et al.*⁷ show zone boundary phonon softening and a ~ 287 K transition, where an R point peak also appears in single crystal diffraction. No incommensurability or slow dynamics were observed and a perfectly ordered I4/mcm structure was inferred. In powder diffraction an R point peak was observed below 280 K. Following the publication of Kim *et al.*¹² showing a long-wavelength incommensurate structure, Ellis reiterated their viewpoint³². Allietta *et al.*¹⁰ instead describe disordering from (235 to 282) K, with long range parts of their pair distribution function showing a cubic structure along with a local tetragonal structure. Splitting was not observed in their powder diffraction data until 215 K. The origin of this discrepancy may be due to defects and disorder that are sample preparation dependent. Goian *et al.*⁹ argue that the existence of Eu^{III} lowers T_N , while O vacancies are hypothesised to change the C-T temperature, and that these differ between samples. O vacancies may also be intrinsically magnetic, as has been shown experimentally for STO ³³. This, combined with the multiple nearby energy minima calculated to be possible by Yang *et al.*³⁴ and Rushchanskii *et al.*³¹, may lead to local disordering of the oxygen tilts. The arguments about the effect of magnetic field on the tilting phonon modes made by

Rushchanskii *et al.* suggest that the response of the tilting transition temperature to magnetic field may show some details of what kind of effects exist in individual samples.

Here we explore the magneto-elastic properties of ETO, and attempt to clarify differing reports regarding its structures and transition temperatures. The broad temperature evolution of the elasticity in ETO has previously been examined^{9,13,35}, as well as a more detailed investigation of the low temperature phase transitions³⁶. Extending the work of Ref. 36, we use a combination of resonant ultrasound spectroscopy with applied magnetic field and stress and SQUID magnetometry to probe the magneto-elastic behavior in specific temperature regimes. RUS spectra have been collected under two different protocols, in fixed field with varying temperature and in fixed temperature with varying field with head designs that lead to either a significant or a near-zero stress being applied to the sample in-situ. Our results provide evidence for obvious differences between samples, unreported elastic anomalies at low temperature in a single crystal and thermal and magnetic history dependent behavior over a broad temperature range. Overall we find that ETO is a system with significantly greater complexity than anticipated.

II. EXPERIMENTAL DETAILS

Two main samples were used in this investigation, a single crystal and a polycrystalline sample. The single crystal sample (hereafter known as SC) is from one of two batches that were grown at Waseda University in a floating zone furnace³ and which were also the source of crystals used by Allieta *et al.*¹⁰, Petrović *et al.*¹¹ and by Spalek^{18,35}. It has T_S of 284 ± 2 K, as determined from specific heat measurements³⁵. The synthesis of this sample is described in detail by Katsufuji and Tokura³ and X-ray diffraction has also been performed^{10,18}, with a small amount ($\sim 1\%$) of $\text{Eu}_2\text{Ti}_2\text{O}_7$ nonmagnetic impurity found to be present. The SC sample used in our experiments was roughly a parallelepiped in shape and had dimensions of $\sim 2.5 \times 2.5 \times 1.5$ mm, with mass 50.8 mg. The primary polycrystalline sample (hereafter referred to as PC1) used in our experiments was an irregularly shaped piece of a sintered pellet with diameter ~ 4.9 mm, greatest thickness 2.0 mm and weighing 148.4 mg. It was prepared by carefully mixing dried Eu_2O_3 (Alfa, 99.99 %) with Ti_2O_3 powder (Alfa, 99.99 %), in a 1:1 ratio in an agate mortar under Ar. The powder was pressed to a pellet and heated in a corundum tube under Ar for 2 d at 1753 K. After cooling to room temperature the sample was ground and heated again for 3 d under the same conditions. ETO samples heated at lower temperatures (< 1623 K) exhibit the structural phase transition at 283 K. In those samples T_S is signaled by a pronounced peak in the heat capacity (see 37). The sample PC1 stems from an early synthesis and is not identical to the one used in Guguchia *et*

*al.*³⁷. A second polycrystalline sample (hereafter known as PC2) has also been measured, with analogous synthesis conditions as PC1, however, using lower heating conditions than applied for PC1.

RUS measurements were performed using purpose built electronics designed by Dr. A. Migliori in Los Alamos, with a maximum applied voltage of 2 V. The design of the RUS head has been described by McKnight *et al.*³⁸, and was attached to the end of a stick lowered into an Oxford Instruments Teslatron PT cryostat equipped with a 14 T superconducting magnet. In this head design, the bottom transducer is fixed in position, but the top transducer is attached to a metal rod that slides vertically in a bore to accommodate the sample, and which rests lightly on it due to its own weight. The material normally used for this sliding rod is stainless steel, but as this is paramagnetic it responds to magnetic field gradients. With this in mind, both stainless steel and copper rods were fabricated and the results obtained with magnetic field in each case were used to deconvolute the effect of magnetic field alone (with a diamagnetic copper rod, known as an H experiment) or the combined effect of an applied stress and applied magnetic field (with a paramagnetic steel rod, known as an $H\sigma$ experiment). As a result of the paramagnetism of the steel rod, the force at a given magnetic field is expected to be inversely proportional to the temperature, but neither the room temperature force nor the temperature dependent force were measured directly and are thus not known to any degree of precision. Spectra were accumulated in programmed sequences of varying temperature at constant field or varying field at constant temperature, and a delay of 20 minutes was enforced within a set tolerance (generally 0.03 K) of each set point to ensure equilibration prior to data collection. For variable field measurements, the magnet was ramped at a rate of ~ 1 T/130 s and a 20 minute dwell was taken at each magnet setpoint. An additional RUS examination of the PC2 sample was also performed in an Orange helium flow cryostat with DRS Modulus II Electronics and a similar head to that used on the Teslatron instrument. 20 minute dwell times were employed in this experiment. Individual resonances in the spectra were analyzed offline using the software package IGOR (Wavemetrics). Fits based on an asymmetric Lorentzian function gave the peak frequency, f , and the width at half height, Δf ; f^2 scales with the combination of elastic constants which determine the resonance and the inverse mechanical quality factor $Q^{-1} = \Delta f/f$ is a measure of acoustic loss.

Magnetometry measurements were performed at the Department of Engineering, University of Cambridge, using a Quantum Designs MPMS XL SQUID magnetometer. The field applied to the SC sample was along the same axis as in the RUS experiments with applied magnetic field. The sequence used for both the SC and PC1 samples involved a zero field cooled (ZFC) run, a “poling” run and a field cooled (FC) run. Between the poling run and the FC run a demagnetisation procedure was

carried out to remove history effects. The ZFC cycle involves cooling without field and measuring the susceptibility with an applied field of 100 Oe. The poling procedure involved cooling the sample in zero field, applying the maximum field of 60 kOe, then measuring the susceptibility while heating in 100 Oe. Finally, for the FC cycle the sample was cooled in 40 kOe and then the susceptibility was measured while heating in 100 Oe, as for the other protocols.

III. RESULTS

Magnetic susceptibility

We have collected magnetic susceptibility data on PC1 and PC2 samples as well as additional SC data to that already reported for this sample³⁶. New measurements on the SC sample were performed in order to examine the effect of a “poling” scheme on the magnetic properties of ETO, for comparison with RUS results from experiments conducted under a similar protocol (figure 1). The most obvious broad observation in the magnetic susceptibility data is that the poled sample has slightly lower susceptibility than either the FC or the ZFC measurements over the temperature range measured, for SC, PC1 and PC2 samples. This may be due to the mechanism of the poling regime, as the magnet is not demagnetized after poling, leaving a small residual field in the instrument that is not completely controlled for. In most aspects, the three samples have broadly similar behavior. An examination of the reciprocal susceptibility shows Curie-Weiss (CW) behavior above T_N , with an (anomalous, namely positive) extrapolated Curie temperature of around (2.2 to 2.5) K in the SC sample, (2.0 to 2.4) K in PC1 and (2.8 to 3.1) K in PC2. The anomalies in the χT data of Caslin *et al.*¹⁴ were not reproduced in our data, possibly because their reported magnitude is close to the noise limit of the data collected here (see Appendix). M-H loops were also gathered at room temperature, but showed perfectly linear paramagnetism.

$T_N \sim 5.6$ K in the SC sample, ~ 5.3 K in the PC1 sample and ~ 5.4 K in the PC2 sample. The subtle break in slope observed near the ab-c spin easy plane-easy axis transition at $\sim (2.6$ to $2.8)$ K in the SC sample (also discussed in Ref. 36) is not evident in the PC1 or PC2 samples. There is, however, a drop in moment below ~ 2.4 K for almost all traces, but whether this is the same phenomenon is unknown. The PC1 and PC2 samples display some FC/ZFC irreversibility and change in slope below 4.6 K, stemming presumably from a small amount of impurity.

Constant field, varying temperature RUS measurement

The capabilities of the recently acquired RUS equipment at Cambridge with in-situ magnetic field allow a thorough examination of the high temperature (cubic-tetragonal) phase transition, T_S , and determination of its stress and field dependence. This is mostly motivated

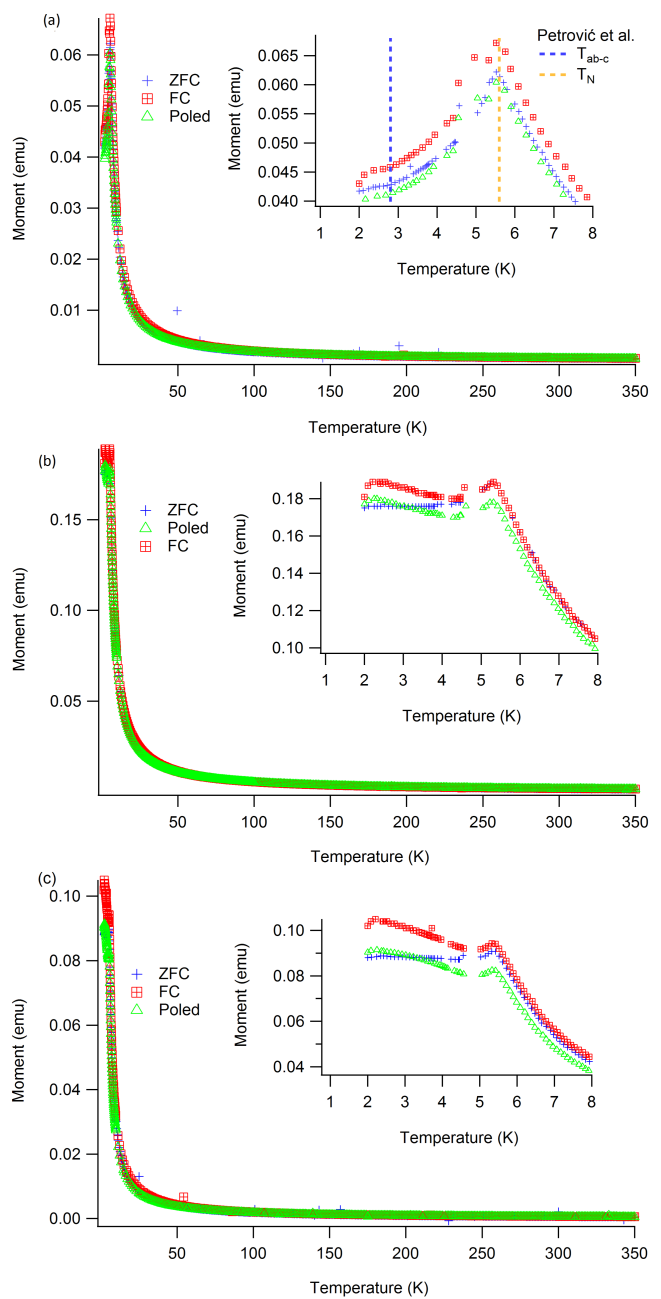


FIG. 1. SQUID magnetometry of (a) SC, (b) PC1 and (c) PC2 samples, with insets showing low temperature behavior

by the report of Guguchia *et al.*³⁷, who showed a clear +4 K shift in the transition temperature (determined by specific heat measurements) under an applied field of 9 T.

In order to examine the nature of the shift of T_S , experiments with applied field and stress ($H\sigma$) were performed on both SC and PC1 samples, while the SC sample was also examined with applied field only (H). To make the experiments with applied field more efficient, measurements were carried out in zero field beforehand to allow the determination of the temperature range over

which the elastic anomaly associated with the transition extends, as well as looking for hysteresis and loss behavior that exists without magnetic modification. While the elastic data of the PC1 sample can be adequately represented with a single plot of f^2 vs temperature, the SC sample has the additional feature of being anisotropic with regard to shear stress. If the domains of the tetragonal structure are randomly oriented, then the average symmetry of the crystal will be cubic. As the resonances in the frequency regime are dominated by shear motions, due to their lower stiffness, the resonance frequencies should be determined predominantly by different proportions of the shear elastic constants.

The two symmetry adapted cubic elastic shear moduli are $C_{11} - C_{12}$ and C_{44} . These relate to the “tetragonal” strain $\frac{1}{\sqrt{3}}(2e_3 - e_1 - e_2)$ and the “rhombohedral” strain e_4 respectively. As the tetragonal strain refers to a macroscopic distortion of the cubic collection of tetragonal twins through movement of twin walls (generating a tetragonally distorted macroscopic crystal), it is expected that “ $C_{11} - C_{12}$ ” mirrors the effect of microstructural features, such as pinning or freezing of twin walls. e_4 is strictly zero in both the ideal tetragonal and cubic phases and thus “ C_{44} ” should be independent of a fully ordered microstructure. Inverted commas are used to emphasize that these elastic constants are cubic averages of the tetragonal elastic constants, as also discussed in Ref. 36. Formally, individual resonances are mixtures of shear modes along with some small contribution from breathing motions that are dependent on the bulk modulus. However, the assignment of the majority character of a given resonance is an effective approach for samples with irregular shapes, for which mode assignments cannot be made definitively.

Two different trends in elastic behavior were identified in the SC sample, one which shows softening as T_S is approached from below and one that shows stiffening. These two trends are related to the two effectively cubic shear moduli below T_S . Based on results for SrTiO_3 ³⁹, the peaks that show softening as T_S is approached from below are assumed to correspond primarily to “ $C_{11} - C_{12}$ ” while those that show stiffening are related to “ C_{44} ”.

The results of experiments examining the overall transition behavior are shown for the PC1 sample for a $H\sigma$ experiment (figure 2) and for both “ C_{44} ” type peaks (which stiffen as the transition is approached from below) and “($C_{11} - C_{12}$)” type peaks (which soften as the transition is approached from below) for the SC sample, again for a $H\sigma$ experiment (figures 3 and 4). The complete transformation in the PC1 sample takes place over a significantly larger temperature interval than that in the SC sample. A very similar level of softening, $\sim 30\%$, is observed through the transition in both samples.

$H\sigma$ runs, with applied magnetic fields and stress, were carried out across the entire temperature range (for the SC sample, figure 3 - figure 4), and then in small steps between 278 and 300 K (for the SC sample, next section, figures 7 and 8), between 274 and 300 K (for the PC2

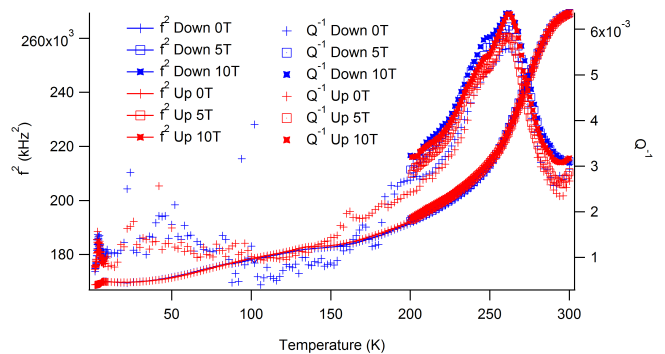


FIG. 2. Analyzed RUS data for 0 T, 5 T and 10 T for $H\sigma$ runs from 1.5 K to 300 K for the PC1 sample.

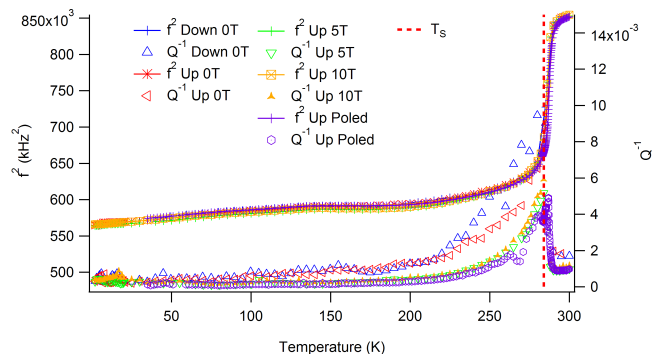


FIG. 3. Analyzed RUS data for 0 T, 5 T, 10 T and “poled” $H\sigma$ runs from 1.5 K to 300 K for a “ C_{44} ” peak in the SC sample at 920 kHz at room temperature. T_S is 284 K and is taken from Ref. 18.

sample, next section, figure 10) or above 200 K (for the PC1 sample, next section, figure 9). A poling process is also shown in figures 3 and 4, which was similar to the one for the magnetization measurements described above, but with the addition of applied stress from the steel transducer-rod, in which the sample was cooled to 3 K in zero applied field, a field of 14 T was applied for 30 minutes, followed by heating in zero field.

The major softening in the SC sample occurs between 290 K and 284 K (figures 3 and 4) along with a clear broad maximum in Q^{-1} . The 284 K limit correlates well with the previously reported behavior from heat capacity measurements, with phase transition temperatures of (283 to 284) K^{10,18,35}. In contrast, the comparable level of softening in the PC1 sample occurs over the range (295 to 200) K (figure 2), with a distinct break in slope of softening and peaks in Q^{-1} between 250 and 260 K. The breadth (with respect to temperature) of the peak in the elastic dissipation associated with the transition in the PC1 sample is ~ 2 times that of the SC, and occurs at a lower temperature. Furthermore, the apparent second peak in the elastic dissipation in PC1 has not been seen in the SC sample. Note that hysteresis exists between

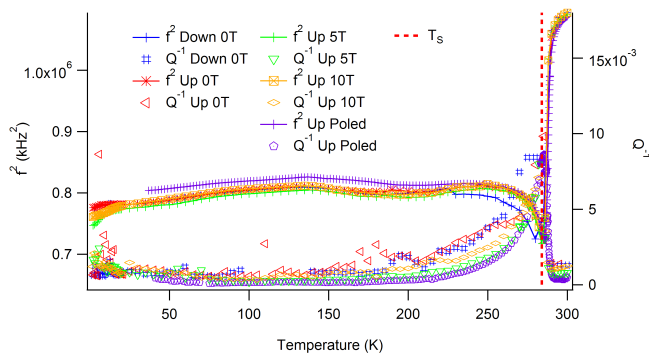


FIG. 4. Analyzed RUS data for 0 T, 5 T, 10 T and “poled” $H\sigma$ runs from 1.5 K to 300 K for a “ $(C_{11} - C_{12})$ ” peak in the SC sample at 1040 kHz at room temperature. T_S is 284 K and is taken from Ref. 18.

the heating and cooling cycles of “ $(C_{11} - C_{12})$ ” in the SC sample between ~ 275 K and 220 K (figure 4), which is absent in “ C_{44} ” (figure 3).

For both SC and PC1 samples, the behavior of the high temperature phase transition with field and stress was quantified. The data shown (figures 3 and 4) for full temperature $H\sigma$ runs in up to 10 T magnetic field do not show the signature of a large shift in the transition temperature for the SC sample. This data was, however, only collected every 5 K for the zero field measurement and every 2 K for the 5 T and 10 T measurements. Nonetheless, a small shift in the elastic softening curves is clear and is downward by ~ 0.5 K under 5 T and unchanged between 5 T and 10 T. This is in contrast to that reported by Guguchia *et al.*³⁷, who find a 4 K shift upward for T_S , predominantly taking place between 3 T and 9 T. A slight increase in softening in the SC sample, particularly for “ $(C_{11} - C_{12})$ ”, is observed with applied field and stress below 250 K, with 5 T yielding the greatest softening.

The softening is clearly interrupted by a local maximum in f^2 at ~ 140 K, followed by a further softening of $\sim 7\%$ in the PC1 sample and 3% in the SC sample (see Appendix for a more detailed view of this temperature region in both SC and PC1 samples). Furthermore, Q^{-1} increases below ~ 60 K, particularly relating to “ $(C_{11} - C_{12})$ ”. Below this temperature, the mechanical losses are enhanced for “ $(C_{11} - C_{12})$ ” relative to “ C_{44} ”.

H runs were also gathered for the SC sample in order to separate the effect of applied stress to the sample. This was performed both in zero applied field and in a 5 T field (figure 5). Instrumental artifacts made measurement of Q^{-1} somewhat unreliable between 50 K and 250 K for the zero field data and for the cooling data in 5 T, but the heating data at 5 T show low values of Q^{-1} in the region of 10^{-4} . Broadly, the zero field data reproduces what is observed in the $H\sigma$ experiments, while the most obvious difference between the $H\sigma$ and the H 5 T data is the effectively complete elimination of any anomaly

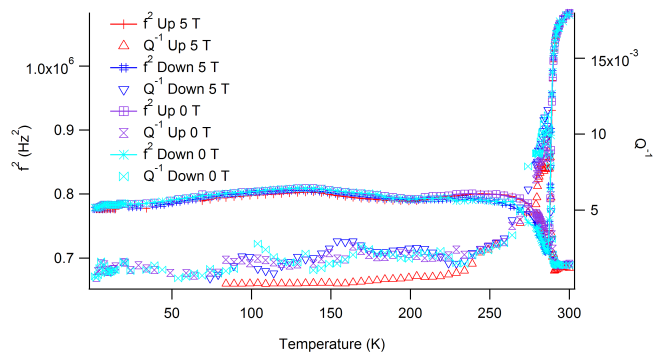


FIG. 5. Analyzed RUS data for 0 T and 5 T H runs from 1.5 K to 300 K for a “ $(C_{11} - C_{12})$ ” peak in the SC sample at 1040 kHz at room temperature. Note that Q^{-1} data between 50 K and 250 K for all traces except 5 T and heating were subject to significant instrumental noise and are thus unreliable.

associated with T_N in the H measurement. The thermal hysteresis evident in “ $(C_{11} - C_{12})$ ” between 250 K and T_S is also seen here for both 0 T and 5 T applied field, while T_S itself is shifted to slightly higher temperature than in the 0 T $H\sigma$ case in both H measurements, as further discussed below.

Examination of T_S

A more thorough examination was carried out for the C-T phase transition in the SC sample with $H\sigma$ runs through the transition in 0.1 K steps and in fields of 5 T, 10 T and 14 T. These runs did not cover the complete temperature range down to 1.5 K, but were instead taken between 278 and 295 K. Temperature steps were taken with 0.5 K intervals in the same range for both of the 0 T and 5 T H full temperature range measurements described above, to enable comparison. “ C_{44} ” and “ $(C_{11} - C_{12})$ ” type peaks collected in $H\sigma$ configuration are shown in figures 7 and 8. There is a clear peak in Q^{-1} at ~ 284.9 K, which can be used as a proxy for shifts in the phase transition temperature itself, and a more subtle peak at ~ 286.5 K, which must correspond to the onset of some kind of dynamic behavior on cooling in the ~ 1 MHz frequency range. In the $H\sigma$ experiment, at a field of 5 T a 0.4 K shift of the elastic anomaly to lower temperature takes place, which is reflected in both the frequencies and in the position of the Q^{-1} anomaly at ~ 284 K. Effectively there is no change of T_S between 5 T and 14 T, with all traces superimposing on one another. A very small hysteresis seen in the data without applied field at T_S itself is suppressed by fields of 5 T or more and their associated stresses. The suppression of the loss seen in the complete temperature runs reported previously³⁶ is not observed. The “ $(C_{11} - C_{12})$ ” peak, in a $H\sigma$ run, exhibits a small hysteresis below 284 K with and without applied field, with almost exactly coincident values of f^2 on heating and cooling for each field value. The H measurements show a roughly 1 K hysteresis, be-

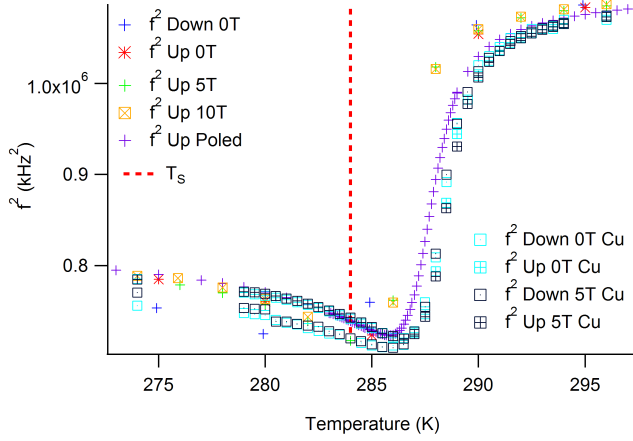


FIG. 6. Analyzed RUS data for 0 T, 5 T, 10 T and “poled” $H\sigma$ runs through T_S for a “($C_{11} - C_{12}$)” peak in the SC sample at 1040 kHz at room temperature along with H -run heating and cooling data at 0 T and 5 T. T_S is 284 K and is taken from Ref. 18. Note that sparse markers (1 marker per 3 data points) are used on the f^2 curves.

tween 285.5 K on cooling and 286.5 K on heating, in the position of the frequency minimum in “($C_{11} - C_{12}$)” at both 0 T and 5 T. In this case, there is no apparent difference between the 0 T and 5 T data in either f^2 or Q^{-1} , suggesting differences observed in the $H\sigma$ measurement must be due to applied stress. A comparison between the $H\sigma$ data, the H data and the “poled” $H\sigma$ data (discussed further below) near T_S is given in figure 6.

Similar behavior to that seen in the SC sample is observed in $H\sigma$ measurements on the PC1 sample, with applied field up to 10 T. See Figure 9 for a detailed view of the T_S region in the PC1 sample. Contrary to what is seen in the SC sample, however, very small stiffening takes place below ~ 255 K for > 5 T, along with a small increase in mechanical loss. A hysteresis of ~ 1 K remains in the PC1 sample with field, while a more significant downward shift of the entire curve by ~ 2 K takes place for both 5 T and 10 T.

The PC2 sample dataset (in the other RUS instrument described in the experimental section) had insufficient resolution at low temperatures to detect the features around 140 K, but as shown in Figure 10, the behaviour near T_S is sharp, and analogous to that of the SC sample. The majority of softening occurs between ~ 279 K and ~ 287 K, with a prominent peak in loss at ~ 276 K. The transition temperature derived from specific heat measurements (Bussmann-Holder, unpublished) is 282 K and is shown as a broken line.

Low temperature

The low temperature behavior of the PC1 sample exhibits only one loss peak (see figure 11) with varying temperature, as opposed to three peaks seen in our SC sample (see figure 12 and ref. 36). The break in slope of the elastic modulus in the PC1 sample resembles the one

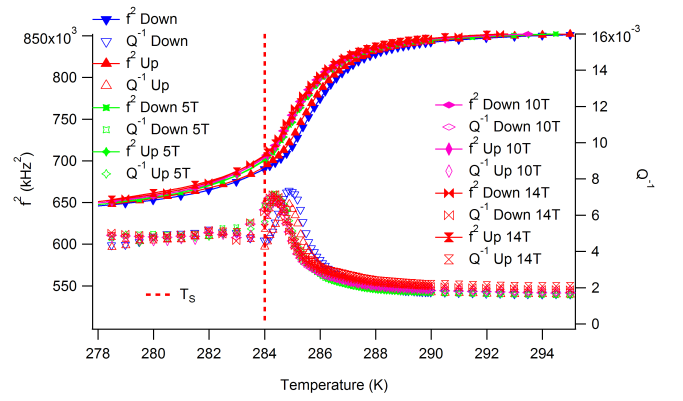


FIG. 7. Analyzed RUS data for 0 T, 5 T, 10 T and 14 T $H\sigma$ runs through T_S for a “ C_{44} ” peak in the SC sample at 920 kHz at room temperature. T_S is 284 K and is taken from Ref. 18. Note that sparse markers (1 marker per 3 data points) are used on the f^2 curves.

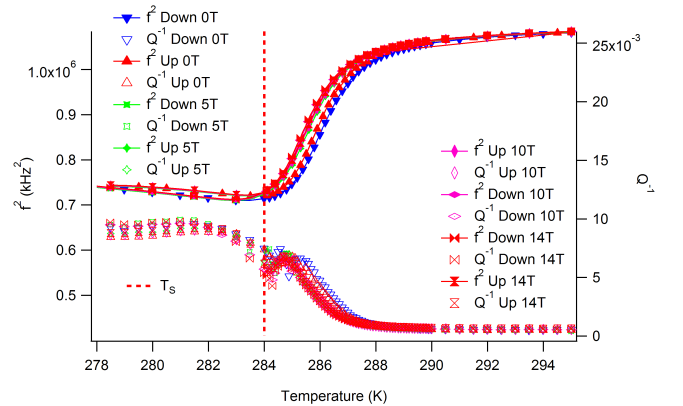


FIG. 8. Analyzed RUS data for 0 T, 5 T, 10 T and 14 T $H\sigma$ runs through T_S for a “($C_{11} - C_{12}$)” peak in the SC sample at 1040 kHz at room temperature. T_S is 284 K and is taken from Ref. 18. Note that sparse markers (1 marker per 3 data points) are used on the f^2 curves.

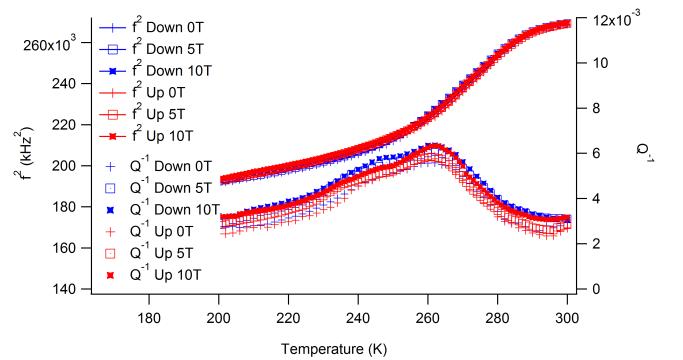


FIG. 9. Analyzed RUS data for 0 T, 5 T and 10 T $H\sigma$ runs through T_S for the PC1 sample.

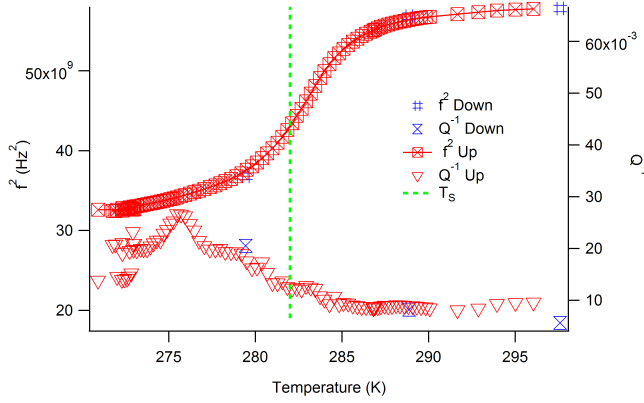


FIG. 10. Analyzed RUS data for a 0 T run through T_S for the PC2 sample. T_S is 282 K and is taken from unpublished data of Bussmann-Holder.

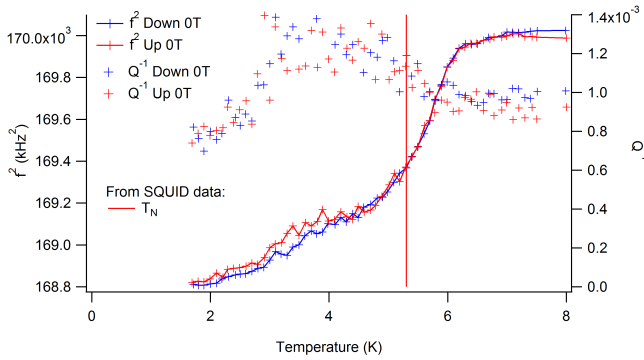


FIG. 11. Analyzed RUS data between 1.5 K and 8 K in the PC1 sample.

in the SC sample, at ~ 6 K, while there is a further break in the slope of frequency at ~ 5 K, with an associated peak in the loss. The loss of configurational information in the polycrystalline sample would be expected to partially suppress and smear these signatures, and this may also explain the difference between the polycrystalline samples and the SC sample in figure 1.

The effect of stress and magnetic field and of magnetic field alone on the low temperature behaviour of “ $(C_{11} - C_{12})$ ” in the SC sample are represented in figure 13. It is obvious that the zero field data for both $H\sigma$ and H measurements are very similar. In the H measurement at 5 T, the softening signature of T_N is effectively completely suppressed, while for the $H\sigma$ experiment softening is seen with an increasing onset temperature of around 13 K at 5 T and 20 K at 10 T. Note that the applied stress is rapidly changing at these low temperatures and has not been quantified or calibrated, but if it varies at $1/T$ it will be 10 times larger at 2 K than at 20 K.

Poled RUS

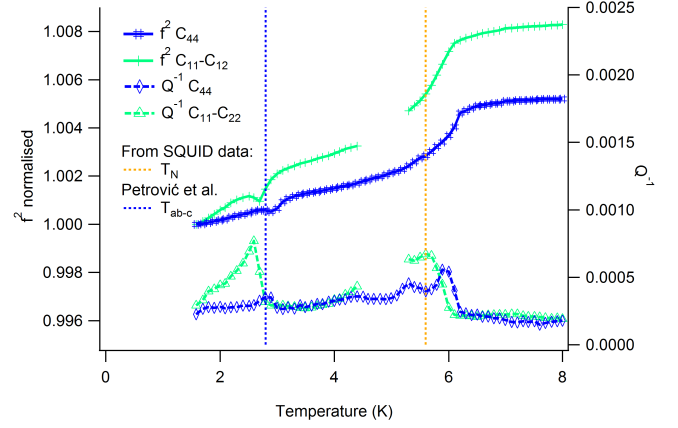


FIG. 12. Analyzed RUS data between 1.5 K and 8 K in the SC sample.

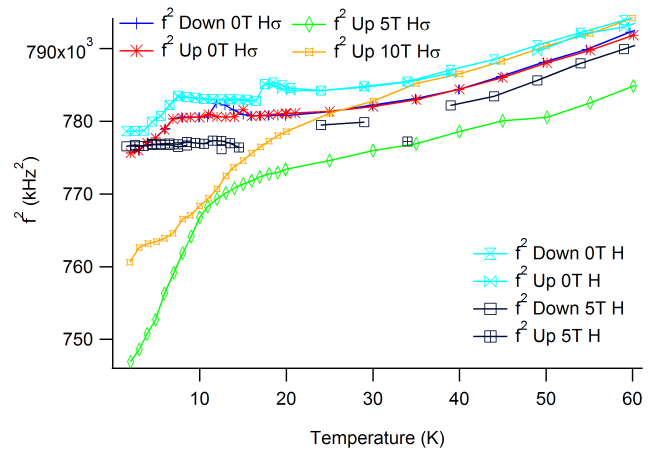


FIG. 13. Analyzed RUS data between 1.5 K and 60 K in the SC sample in both $H\sigma$ configuration, with 5 T and 10 T applied fields, and H configuration, with 5 T applied field

A zero-field, variable-temperature investigation was performed on the SC sample in $H\sigma$ configuration, in order to investigate the effect of simultaneous magnetic and stress poling at low temperatures and its effects on T_S . Under this condition, the softening in the SC sample is shifted up by ~ 1.9 K. The peak in the mechanical loss at 285 K in “ C_{44} ” splits into two at 285 K and 287 K in the poled measurement. Cycling the temperature through the transition creates jumps between temperature dependent curves reminiscent of the poled and unpoled state (see figure 16), with associated loss peaks. Further measurements both without and with field, in the $H\sigma$ configuration, did not recover the unpoled-like state, and sometimes an intermediate state was also observed. Noting that the sample was then stored at room temperature, and that 300 K was insufficient to remove memory in the sample, the poled state may have remained for the subsequent H measurements. The poled sample ex-

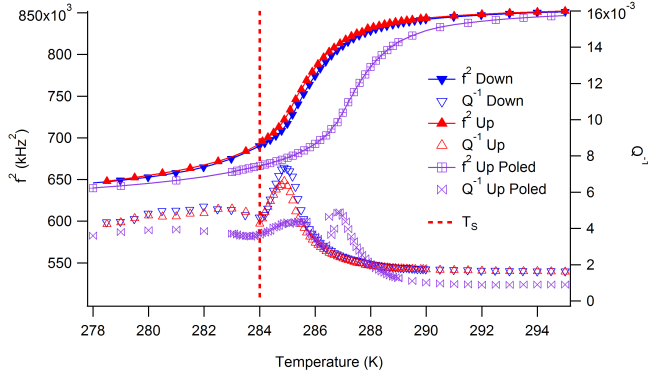


FIG. 14. Analyzed RUS data for “unpoled” and “poled” runs through T_S for a “ C_{44} ” peak in the SC sample at 920 kHz at room temperature. T_S is 284 K and is taken from Ref. 18. Note that sparse markers (1 marker per 2 data points) are used on the f^2 curves.

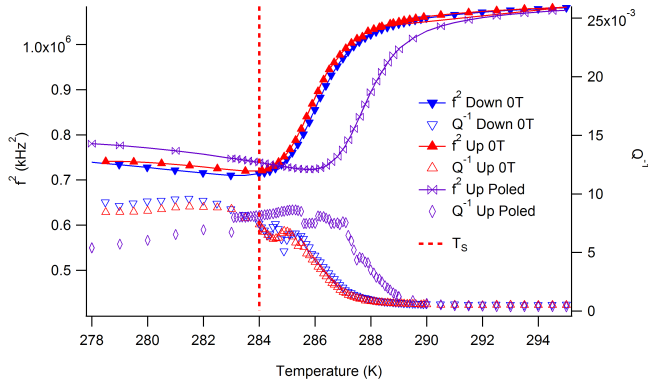


FIG. 15. Analyzed RUS data for “unpoled” and “poled” runs through T_S for a “ $(C_{11} - C_{12})$ ” peak in the SC sample at 1040 kHz at room temperature. T_S is 284 K and is taken from Ref. 18. Note that sparse markers (1 marker per 2 data points) are used on the f^2 curves.

hibited significantly lower loss below T_S as compared to the unpoled samples with respect to both “ C_{44} ” and “ $(C_{11} - C_{12})$ ” (figures 14 and 15), while “ C_{44} ” peak retained significantly lower loss above T_S , as can be seen in figure 14.

Constant temperature, variable magnetic field RUS hysteresis loops

A number of experiments were carried out in order to monitor the response of the sample to varying magnetic field at constant temperature, both in $H\sigma$ and H modes. Again, different regimes are evident depending on the sample temperature and whether or not stress is applied to the sample through the transducer-rods. “ $(C_{11} - C_{12})$ ” data were collected on a peak with a frequency of ~ 700 kHz at room temperature that shows softening upon approaching T_S from below, while “ C_{44} ” data

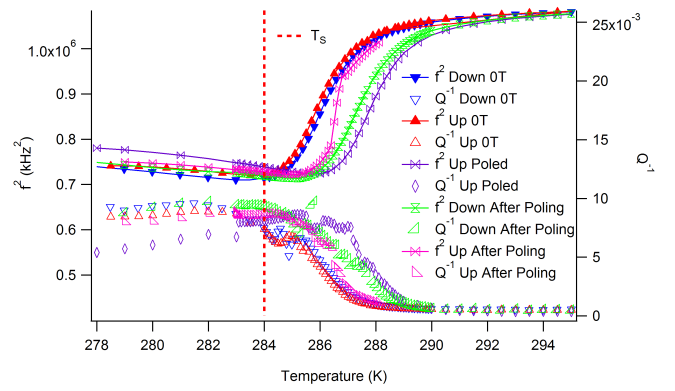


FIG. 16. Analyzed RUS data near T_S for 0 T and “poled” runs, along with the recovery after poling for “ $(C_{11} - C_{12})$ ” in the SC sample. T_S is 284 K and is taken from Ref. 18.

relate to a peak at ~ 920 kHz at room temperature that shows stiffening as T_S is approached from below.

The results at low temperature are closely related to those in³⁶, which did not include a discussion of the applied stress. The “ C_{44} ” type peak in that study could not be traced in the full temperature range investigated here. For this reason the new 920 kHz peak was chosen for the present analysis. Nonetheless, the peak selected in Ref. 36 has the advantage of good amplitude under no applied field, and thus the data given there are more relevant for the true (0 to 1) T behavior at lower temperatures and in the $H\sigma$ configuration. Data shown in this section are normalized to the first point in the series. Any hysteresis is shown by a data point that is not unity at the lowest field indicated for that series, and this will be the final point measured as the field is decreased. Where a given field/frequency combination could not be measured, the results have been normalized to the next available point as the field was increased.

288 K to 295 K

At high temperatures and in $H\sigma$ mode (above T_S), the main feature is nonlinear softening with increasing field and stress, with a concurrent increase in the mechanical loss, Q^{-1} . Near T_S , this softening and the increasing loss had a plateau between ~ 3 T and 7 T, and then increased significantly up to the maximum 14 T field, as shown in figure 17. At 288 K, a ~ 2 % softening by 3 T, together with an additional 5 % softening between 7 T and 14 T takes place. The loss plateaus are 40 % greater than the initial loss from (3 to 7) T and these increase to ~ 130 % by 14 T. A significant hysteresis is observed upon returning to zero field, with a residual 2.5 % softening of f^2 and a 35 % increase in Q^{-1} . This effect is somewhat counter intuitive, since the magnetic field and stress would be expected to drive the system further away from the transition above T_S on the basis of the constant field, varying temperature measurements. At higher temperatures (see Appendix), a similar shape to that seen

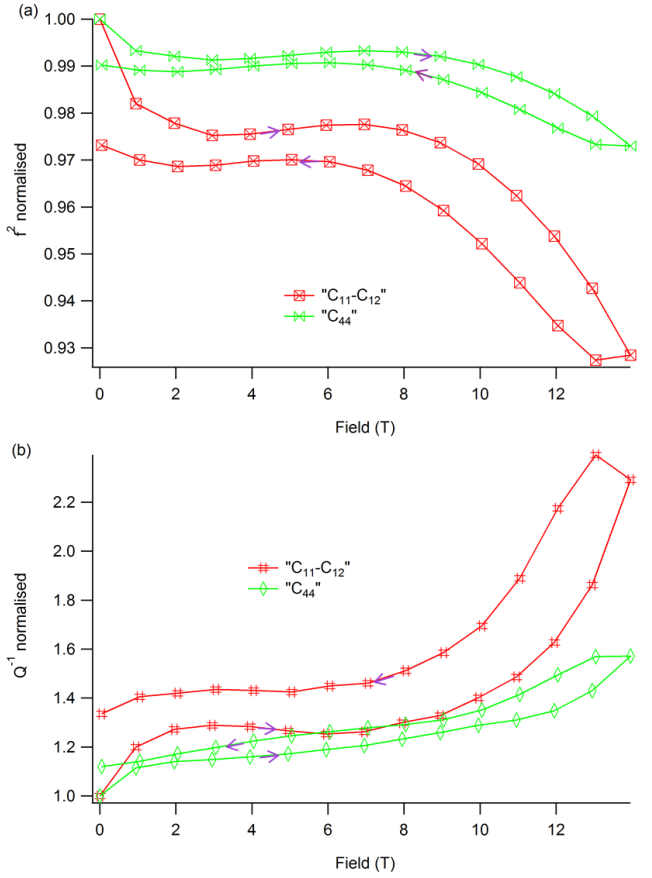


FIG. 17. Magnetic field dependent analyzed RUS data at 288 K, between 0 T and 14 T for the SC sample, in $H\sigma$ configuration

at 288 K is found, but with some stiffening being also present. Note that at 295 K (see Appendix) the response to field is slightly larger for " C_{44} " than for " $(C_{11} - C_{12})$ ", the opposite of that observed at 288 K. An examination of the same temperature range in H configuration, however, showed no appreciable response to magnetic field, implying that much of what was found in $H\sigma$ mode was caused by the applied stress.

215 K to 284 K

At 284 K the softening has vanished and an intermediate temperature regime sets in, which persists to temperatures between 215 K and 170 K (figure 18 and Appendix). In this intermediate regime, the sample stiffens with increasing field and stress and then effectively saturates, with little change in f^2 on lowering the field, resulting in a hysteresis. This is 5 times larger for " $(C_{11} - C_{12})$ " peaks than for " C_{44} ". Furthermore, the " C_{44} " peaks partially lower their frequency upon reducing the field while the " $(C_{11} - C_{12})$ " peaks do not. In this regime, the Q^{-1} values decrease with increasing field and recover with decreasing field, with a hysteresis of $\sim 15\%$ for most " $(C_{11} - C_{12})$ " data. Again, the " C_{44} " peaks show a considerably reduced hysteresis in Q^{-1} of $\sim 5\%$. This be-

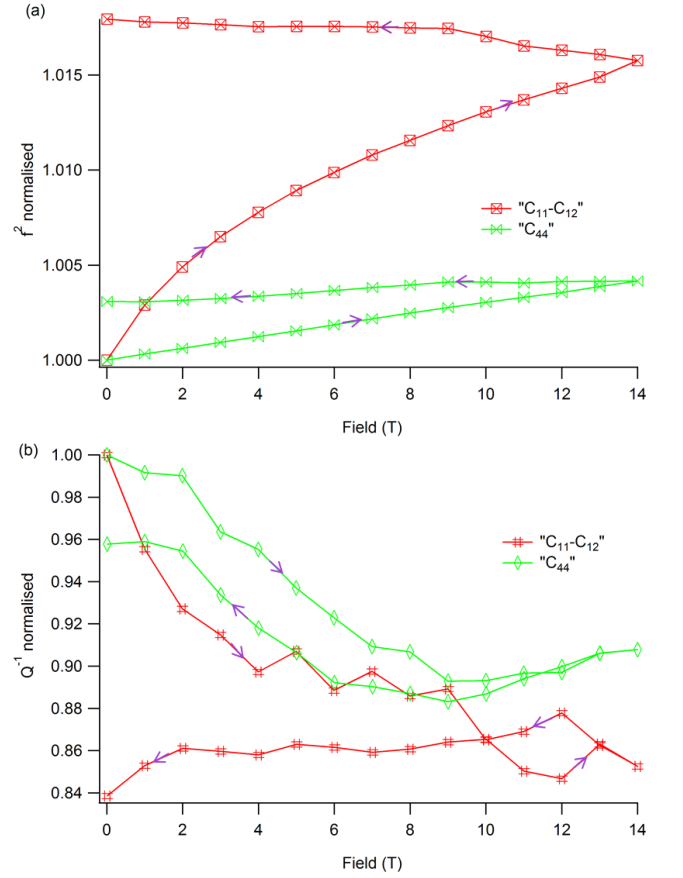


FIG. 18. Magnetic field dependent analyzed RUS data at 245 K, between 0 T and 14 T for the SC sample, in $H\sigma$ configuration

havior is time dependent, displaying increased changes in both f^2 and Q^{-1} with time at particular temperatures and fields. The significant jump in the frequency data for 215 K, in particular those collected for a " $(C_{11} - C_{12})$ " type peak (see Appendix), is due to an instrumental hang up of three days caused by a small (~ 0.1 K) instability in temperature control. The drop in the " C_{44} " loss measurement at zero field at the same temperature appears to have the same origin.

50 K to 170 K

From 170 K to 50 K, a pattern of slight stiffening with field and stress emerges in the $H\sigma$ experiment, and almost complete relaxation sets in upon removal of the field (figures 19 and 20 and Appendix). There are significant increases in Q^{-1} with applied field, reaching a maximum increase of $\sim 100\%$ at 14 T and 110 K for " $(C_{11} - C_{12})$ " and at 80 K for " C_{44} ". Above and below this temperature, the changes in Q^{-1} with field are smaller, with a residual increase of (10 to 20) %. The time dependence seen between 215 K and 284 K is also at least an order of magnitude smaller here.

An examination of the above two temperature ranges in the H configuration shows a time-dependent relaxation

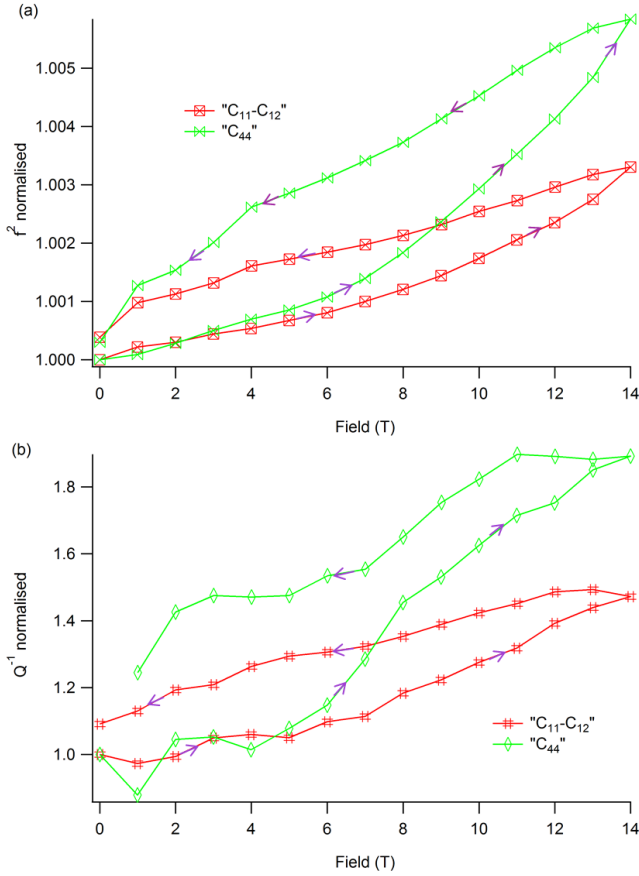


FIG. 19. Magnetic field dependent analyzed RUS data at 170 K, between 0 T and 14 T for the SC sample, in $H\sigma$ configuration

of the measured properties at 245 K and 170 K, but no relationship to magnetic field. This can be clearly identified for various peaks in figure 21. The shift with time decreases markedly with decreasing temperature and no distinct relaxation is seen at 110 K. Additional dwell time between the first and second data point at 245 K due to a software-related fault has been estimated at 2.4 hours based on log information. The exact dwell time at each point is unknown, caused by a temperature reporting error occasionally resetting the counter, but the values given in the figure are believed to be relatively accurate.

3 K to 20 K

For the lowest temperature regions, near and below the Néel point, the hysteresis and time dependence effectively disappears, and new field and stress-induced anomalies take place (see figures 22, 23 and Appendix) in the $H\sigma$ experiment. Many of these peaks do not show enough amplitude for fitting at 0 T and normalization has been performed for peaks at the first available data point, but the effect of the spin flop between 0 T and 2 T on other peaks has been investigated in detail in Ref. 36, although without interpretation of the effect of stress due to the head design. Obviously different be-

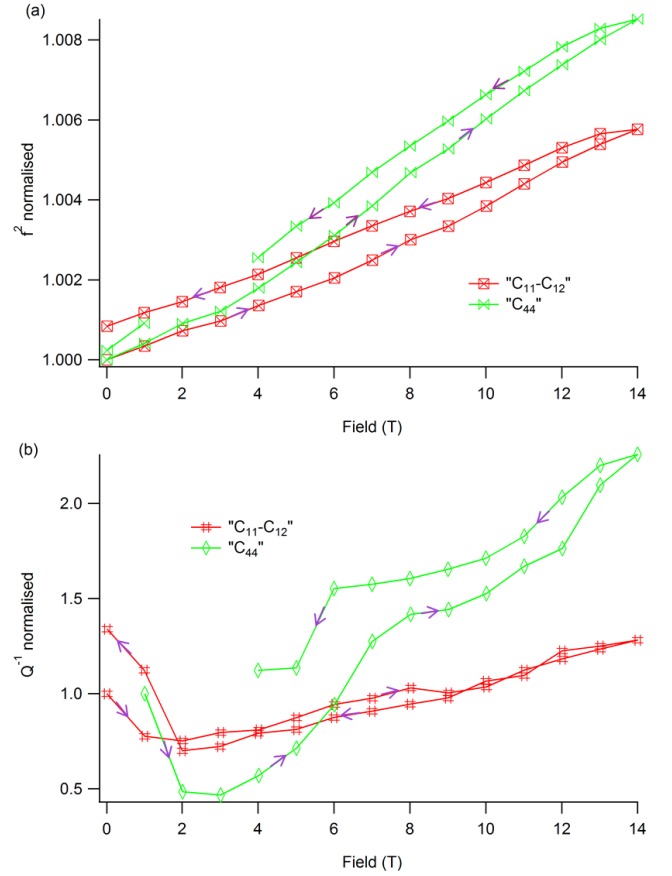


FIG. 20. Magnetic field dependent analyzed RUS data at 80 K, between 0 T and 14 T for the SC sample, in $H\sigma$ configuration

haviour is exhibited by “ $(C_{11} - C_{12})$ ” peaks and “ C_{44} ” peaks from 20 K down, as is expected from the changes at low temperature from the full temperature runs (figures 22 and 23 and Appendix). “ C_{44} ” shows a frequency minimum between 20 K and 5 K decreasing between 3 T and 0 T at 5 K. “ $(C_{11} - C_{12})$ ” exhibits a plateau and softening at higher fields, with critical fields similar to those in “ C_{44} ”. An additional high field/stress anomaly is evident in “ C_{44} ” at 10 K (see Appendix), analogous to that in Ref. 36. The plateau in “ $(C_{11} - C_{12})$ ” followed by softening is also apparent below T_N , at 5 K, 4 K and 3 K (see figure 23 and Appendix), but in this region the turning point increases in critical field/stress with decreasing temperature rather than decreasing as it did above T_N .

For the lowest temperature regions, below 20 K, in the H configuration, the previously analysed peak had insufficient amplitude for the fitting performed above. Nonetheless, it is clear from examining peaks that have sufficient amplitude (see figure 24 and Appendix) that the magnetic field now has a significant influence on the elastic properties, with substantial changes in peak frequency that return on removal of the magnetic field. Examining the behaviour of these peaks at higher tem-

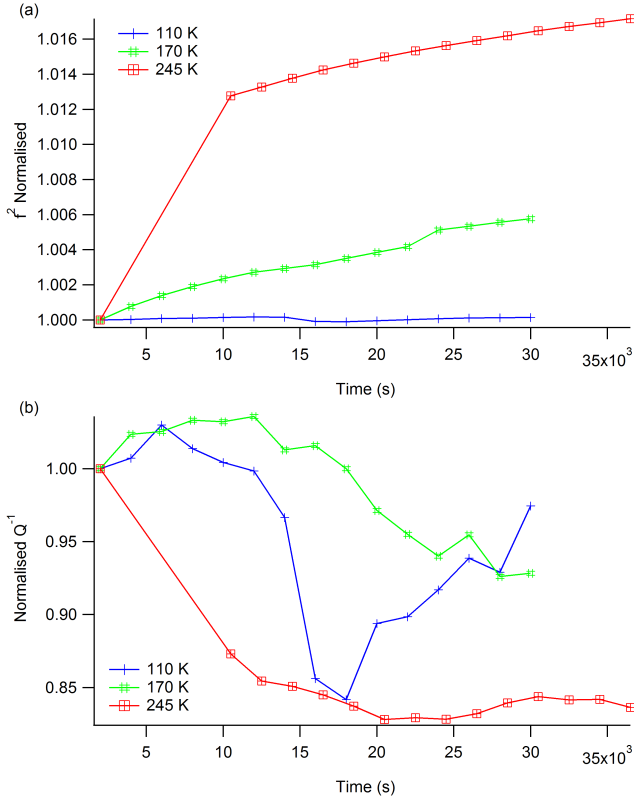


FIG. 21. Magnetic field dependent analyzed RUS data at 110 K, 170 K and 245 K, between 0 T and 14 T for the SC sample, in H configuration, with the bottom axis reflecting dwell time, with the field from (0 to 14 to 0) T as time increases

peratures shows that they exhibit a mixture of both “ $(C_{11} - C_{12})$ ” and “ C_{44} ” character, yielding a superposition of each of those peaks. It is nonetheless clear (see Appendix) that peaks show a strong effect between 0 T and 2 T at lower temperatures and that the trend at 2 T and above changes from stiffening with increasing field above 10 K to a plateau or slight softening with increasing field at 5 K and 3 K. The specific turning points in the figures are as follows. At 15 K there are jumps in f between 0 T and 2 T and 6 T and 8 T, with softening from 8 T to 14 T. At 10 K the behaviour is difficult to follow, but has a maximum in f somewhere between 4 and 8 T with some softening up to 14 T. At 5 K there are jumps in f between 0 T and 2 T and between 2 T and 4 T, with slight softening from 4 T to 14 T. At 3 K a jump in f between 0 T and 2 T takes place with slight softening from 2 T to 14 T.

IV. DISCUSSION

The results presented above and in the appendix show a number of trends in the magneto-elastic response of ETO and allow attribution of aspects of their origin. At

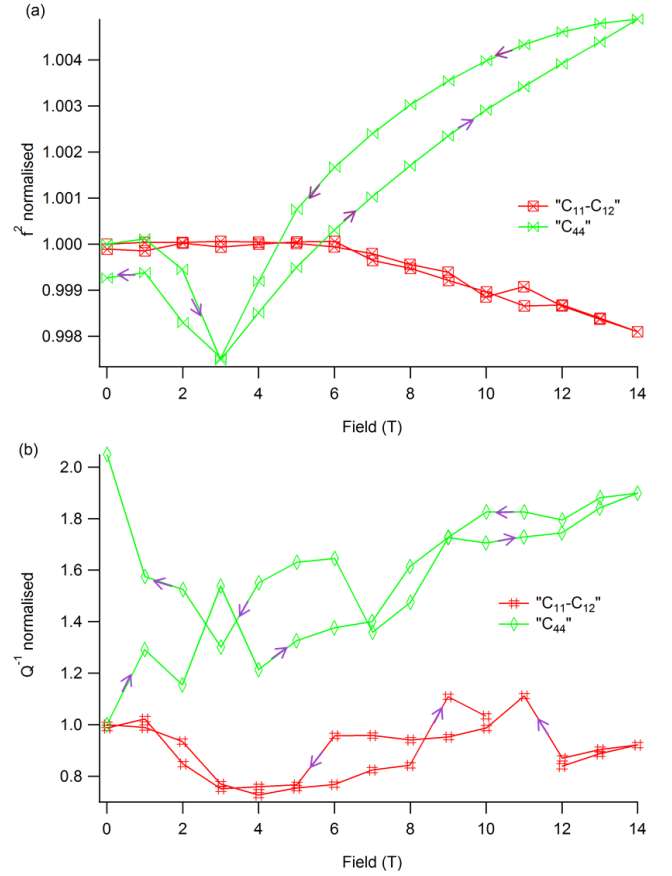


FIG. 22. Magnetic field dependent analyzed RUS data at 20 K, between 0 T and 14 T for the SC sample, in $H\sigma$ configuration

the most superficial level, all the samples exhibit elastic softening and acoustic losses dominated by the influence of the (improper ferroelastic) C-T transition driven by octahedral tilting. In particular, there is softening by $\sim(30$ to $40)$ % which occurs mainly in a small temperature interval above and through T_S and this is accompanied by an increase in acoustic loss. In detail, however, and from the data collected in H and $H\sigma$ configurations, this simple view does not provide a complete explanation of the overall elastic and anelastic behaviour. We argue that both metastability and defects (in the form of vacancies, stacking faulting, domain boundaries or other deviations from ideal crystallinity) have an important influence in ETO, raising questions with respect to the absolute concentration of defects and their effect on the coupling and phase transition behaviour. Following Goian et al.⁹ and Kennedy et al.⁴⁰, and based on the otherwise similar preparation of the samples, particularly PC1 and PC2, variations in defect concentration are believed to contribute to the large differences seen between the samples described here.

The octahedral tilting transition is associated with a softening of $\sim 30\%$ over 5 K in the SC sample (figures

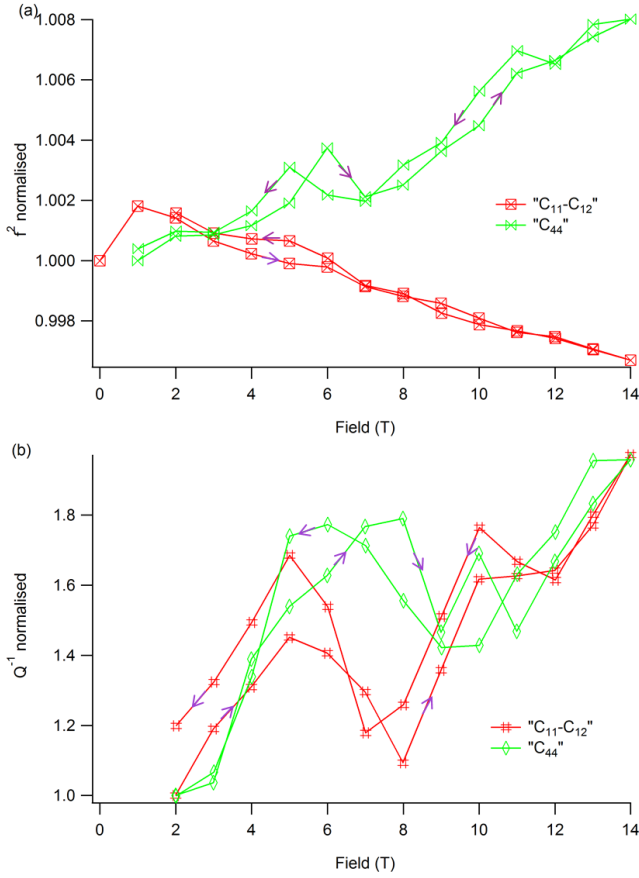


FIG. 23. Magnetic field dependent analyzed RUS data at 5 K, between 0 T and 14 T for the SC sample, in $H\sigma$ configuration

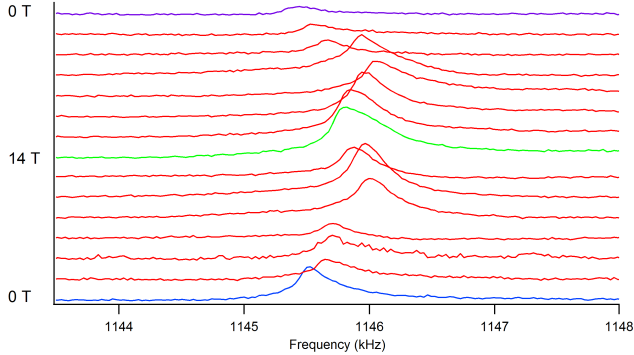


FIG. 24. Magnetic field dependent raw RUS data at 15 K, between 0 T and 14 T for the SC sample, in H configuration

3 and 4) and of $\sim 40\%$ over ~ 10 K in the PC2 sample (figure 10), but the 30% softening in PC1 is smeared through a total range of ~ 100 K (figure 2, and see figure 25)). The latter was sintered at a higher temperature than the others, and might contain a greater number of oxygen vacancies, for instance. This discrepancy between the temperature intervals over which the cubic-tetragonal

transition occurs in PC1 and SC samples is reflected also in differing results reported in the literature, for example between those showing a clear phase transition^{5,32}, those with multiple steps in ordering (*e.g.* Kim *et al.*¹²) and those of Bessas *et al.*¹³, in which no distinct phase transition is observed at all. Discrepancies in elastic and anelastic properties between the three samples used in the present study are summarised in Table I.

One of the most obvious features of the data presented in figures 2-4 is that while many aspects of ETO are analogous to STO, there is a stark distinction in the behaviour of their anelastic properties below T_S . Acoustic loss in STO remains high at all temperatures below T_S and is attributed to highly mobile twin walls, with some additional changes associated with changes in the properties of the walls³⁹. The maximum acoustic loss seen in ETO is approximately half of that taking place in STO³⁹ and, while it is high immediately below the softening interval associated with T_S , it drops rapidly and does not show any form of Debye peak that could be associated with freezing behaviour. This lack of a Debye loss peak indicates that there is no temperature or obvious range of temperatures at which conventional freezing of tetragonal domain wall motion occurs. Rather, the peak in Q^{-1} is associated with the critical point and it appears that the tetragonal twin walls are effectively pinned in ETO almost immediately when they form. The presence of pinning defects has previously been invoked to account for the relatively rapid suppression of elastic losses below T_S ³⁵, and the discovery of a coupling between magnetic field and elastic loss (even in the case of no stress, in the H configuration) implies that some subset of these defects are magnetic in nature.

The time dependence and hysteresis, particularly in constant temperature-variable field measurements, demonstrates non-equilibrium/metastable behaviour. Effective disappearance of the hysteresis below $\sim (215$ to $170)$ K suggests that the defects associated with the hysteretic phenomena have relaxation times in the vicinity of $\sim 10^{-6}$ s in this temperature range and become immobile at lower temperatures. A striking finding is that the magnitude of the suppression of elastic loss in the constant field-variable temperature $H\sigma$ measurements is similar for both " C_{44} " and " $(C_{11} - C_{12})$ " (figures 3 and 4). This clearly demonstrates that the defects responsible for the observed behaviour are able to relax through an e_4 as well as an $e_1 - e_2$ strain and suggests that they are not tetragonal domain walls. The continued suppression of loss up to at least a few degrees above T_S also demonstrates that the defects exist and still couple to a magnetic field even in the high-symmetry structure where tetragonal domain walls are absent.

Evidence for the influence of defects

The influence of magnetic field and stress on T_S

The pronounced peak in Q^{-1} from the SC sample shown in figures 3 and 4 resembles the typical pattern of acoustic loss associated with critical slowing down

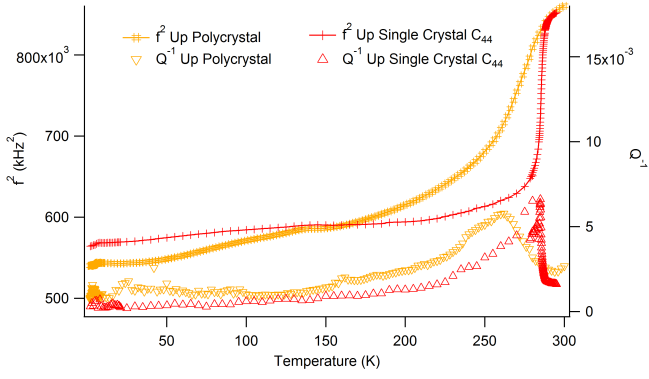


FIG. 25. PC1 and SC comparison, SC uses the contents of two datasets for better resolution at T_S . PC1 f^2 data is scaled to match the SC data near room temperature.

in which coupling of strains occurs with fluctuations of the order parameter that have their maximum relaxation time at $T = T_S$. In detail the peak is more complicated, with the actual maximum occurring at 284.9 K in the SC data (figures 7, 8 and 14). For both PC1 and PC2 the small loss peak occurs just below the independently determined values of T_S , however (figures 9 and 10). The precise origin of this loss behaviour close to T_S is not understood but a combination of classical critical slowing down with some variable microstructure seems to be most likely.

These subtle effects are altered in the SC sample when temperature is changed under constant magnetic field and approximately constant stress in a $H\sigma$ measurement (figures 7 and 8). First, a small downward shift of the softening and loss peak associated with T_S takes place when field and stress are applied. The shift is ~ 0.4 K at 5 T, with no further change between 5 T and 10 T. The measurement without applied stress is independent of the magnetic field, figure 13, and the measured transition temperature in that H experiment is higher than that measured in the $H\sigma$ experiments, suggesting a history dependence to T_S . These results are in contrast to the results reported by Guguchia *et al.*³⁷ of a 4 K upward shift in T_S from specific heat measurements. Secondly, a very small hysteresis between heating and cooling that is present without applied field is suppressed in $H\sigma$ data, but not in H measurements. As noted in the results section, above, the suppression of the loss observed in the complete temperature runs reported previously³⁵ is absent when the magnetic field is only applied in the proximity of the phase transition, suggesting that the effect leading to this lowered loss is due to some magnetostructural response at lower temperatures. The PC1 sample under applied field of up to 10 T in a $H\sigma$ measurement retains a hysteresis of ~ 1 K, and the downward shift of the softening trend appears to be larger, at ~ 2 K in both 5 T and 10 T fields.

When temperature is fixed a few degrees above the

TABLE I. Elastic anomalies and their corresponding temperatures as observed across all samples. Both constant temperature/variable field (CTVF) and constant field/variable temperature (CFVT) anomalies are presented.

Sample	Temperature (K)	Observations
At or near T_S		
SC	287	Peak in Q^{-1} for “ C_{44} ” after poling
SC	285	Peak in Q^{-1} for “ C_{44} ” before poling, shows up slightly also after poling
SC	274-284	Small hysteresis in “ $(C_{11} - C_{12})$ ”
PC2	276	Peak in Q^{-1}
Intermediate temperatures and irreversibility		
SC	288-284	Disappearance of critical softening in CTVF loops
SC	265	Peak in Q^{-1} for “ C_{44} ” after poling
PC1	260	Broad peak in Q^{-1}
PC1	240	Broad peak in Q^{-1}
SC	280-225	Hysteresis in “ $(C_{11} - C_{12})$ ”
SC	<240	Difference between poled and unpoled “ $(C_{11} - C_{12})$ ”
SC	215-170	Disappearance of hysteresis in CTVF loops
The frozen lower temperature state above T_N		
SC	140	Local maximum in f^2
PC1	140	Local maximum in f^2
Magnetic anomalies near and below T_N		
SC	<20	Appearance of distinct anomalies in CTVF loops and separation of CFVT traces for different fields (particularly for “ $(C_{11} - C_{12})$ ”)
SC	6.1	Onset of softening associated with T_N
PC1	6	Onset of softening associated with T_N
SC	5.9-6	Peak in Q^{-1} near T_N
PC1	4	Peak in Q^{-1}
SC	2.3	Peak in Q^{-1} and minimum in f^2

C-T transition and the magnetic field and stress are increased, elastic softening and an increase in Q^{-1} occur for both “ C_{44} ” and “ $(C_{11} - C_{12})$ ” like peaks, although the effect is significantly more pronounced for “ $(C_{11} - C_{12})$ ” (figure 17). These changes would be expected if there is an upward shift of the transition temperature of the form as seen by Guguchia *et al.*³⁷, but application of magnetic field alone in a H measurement does not yield a discernable effect on the elastic moduli either with constant field and varying temperature or constant temperature and varying field. The evolution of the elastic softening and concomitant increase in elastic loss with applied stress in a $H\sigma$ experiment are highly nonlinear, with a plateau around 5 T. The origin of this nonlinearity is un-

clear. The discrepancy between the behaviour observed in constant field/stress with varying temperature and in constant temperature with varying field/stress evidence that the elastic and anelastic properties are history dependent, most likely due to variations in the microstructure and defect distribution. An irreversible change in microstructure is consistent also with hysteresis in the field-sweep measurements, where a residual softening of (1 to 3) % remains after removing the field (figure 17).

The effect of poling

In the poling experiment, the SC sample was cooled to 2 K, a 14 T field was applied for ~ 30 min in a $H\sigma$ configuration. The field was then switched off and elastic behaviour examined in zero field up to room temperature. Under these conditions, T_S was shifted up by ~ 2 K (figures 15 and 16) rather than down by ~ 0.4 K as was observed in the previous constant field-varying temperature scenarios with the same head configuration. Furthermore, cycling the temperature near T_S with zero applied field/stress displayed a “jump” from the poled trends in f^2 and Q^{-1} to the virgin curve approximately half way through the transition. This, however, was not retained upon cooling again from 300 K, with the poled state returning for the cooling curve and the heating curve showing jagged jumping again up to the virgin curve, in an unpredictable and irreproducible way (see figure 16). Application of a field/stress in $H\sigma$ runs through T_S on these poled curves simply yielded a shift of -0.4 K and suppression of the small hysteresis (seen in measurements without applied field), as before, but now relative to the renormalized T_S of the poled sample. From these observations it is clear that magnetic field and stress poling must cause changes in structure which act on the structural transition as an effective internal field. In other words, low temperature poling of ETO results in structural changes that persist up to temperatures just above T_S .

Irreversibility and the intermediate temperature regime

Variations of apparent T_S with the SC sample subjected to changes in temperature in a constant applied field and in a $H\sigma$ configuration yield essentially the same changes in elastic moduli, irrespective of field strength (figures 3 and 4). On the other hand the field and stress cause reductions in the acoustic loss and it was argued previously³⁶ that the changes could not be due to any influence of the field on the configuration of ferroelastic domain walls since these would be expected to modify the effective elastic constants of the whole crystal and apply predominantly to “ $(C_{11} - C_{12})$ ”. The field effect was separated from the stress effect in figure 13 where $H\sigma$ and H measurements were compared. Despite some instrumental artifacts in the H measurements, heating data at 5 T showed Q^{-1} effectively indistinguishable with that observed in the 5 T $H\sigma$ data, suggesting that at least a significant part of the suppression of elastic loss originates from the applied field rather than the applied stress.

Variations with applied field/stress at constant tem-

perature in a $H\sigma$ configuration yield a marked hysteretic behaviour at 245 K (figure 18) and at 284 K, 282 K, 275 K, 215 K (Appendix), related to some aspect of the microstructure being modified by field or stress. This is seen to a much lesser extent at 170 K (figure 19) and 140 K (Appendix) but not at all at 80 K, 20 K or 5 K (figures 20-23). The temperature interval $\sim (150$ to $290)$ K also corresponds to the range in which values of Q^{-1} are above baseline values (figures 2-4), *i.e.* where relaxation times of the defects responsible for the acoustic losses are shorter than $\sim 10^{-6}$ s. By chance, the cryostat controller stalled at 10 T and 215 K for ~ 3 days, and the large jump in f^2 for “ $(C_{11} - C_{12})$ ” (see Appendix) at 11 T is due to this dwell. This suggests a time dependence, in addition to any field/stress dependence and was reproduced in H experiments, as seen in figure 21, which show that effectively the whole relaxation in the $H\sigma$ experiments in this temperature regime is likely to be due to relaxation over time. A trivial lack of thermal equilibration was ruled out by supplementary experiments that verified stiffening in the sample over time whether the setpoint was approached from above or from below in temperature. Stiffening of up to ~ 1 % was found for “ $(C_{11} - C_{12})$ ” peaks and ~ 0.15 % for “ C_{44} ” peaks in a separate 8.5 hour dwell without field at 245 K. This again is consistent with the microstructure depending on the previous thermal history. On this basis, the defects responsible for the acoustic losses appear to become immobile below $\sim (150$ to $200)$ K.

The frozen structure and low temperature behaviour

Below 200 K, the constant temperature, variable magnetic field/stress traces in the $H\sigma$ measurements assume a different character, with significantly smaller maximal stiffening in f^2 , almost zero residual change after removal of the field, a larger response from “ C_{44} ” than “ $(C_{11} - C_{12})$ ” for the first time (indicating that the role of microstructure has become less important than the intrinsic behaviour) and with large increases in Q^{-1} of up to 85 % instead of smaller decreases of around 30 % in the higher temperature regime (figure 19). This behaviour persists down to at least 50 K, before significant changes occur again around 20 K. These effects appear to be related to stress, and the H measurements exhibited basically no relaxation over time, consistent also with the observed lack of hysteresis with applied stress.

As discussed by Spalek *et al.*³⁵, there is a small but distinct maximum in f^2 at ~ 140 K and softening below this point. In the absence of any further structural instabilities, elastic stiffening would be expected with decreasing temperature rather than softening. This correlates with a change from coexisting antiferrodistortive and modulated order to purely modulated antiferrodistortive order reported at around 160 K by Kim *et al.*¹². However, it also correlates with deviations from the classical evolution of the ferroelectric soft mode on cooling observed by Goian *et al.*¹⁶ at ~ 155 K, by Kamba *et al.*⁸ at ~ 113 K and the extrapolated saturation temperature of the Barrett fit to the dielectric data of Katsufuji *et al.*². It is inter-

esting to note that the maximum occurs in both the SC and PC1 samples, despite the significant difference in the softening behaviours seen at their C-T transitions. This implies that whatever disorder is driving the “smearing” of the phase transition in PC1, it has little effect on the cause of the anomalous softening below 140 K.

Low T magnetic anomalies and a possible phase diagram

In the region below 50 K, the constant field/stress, variable temperature data in a $H\sigma$ configuration exhibit a point at which a significant change both in the sign and magnitude of the slope of “ $(C_{11} - C_{12})$ ” (figures 22, 23 and Appendix) takes place. This change in slope occurs at a temperature that increases with increasing field, yielding a $\sim 4\%$ maximal softening at 2 K as compared to that measured without field or stress applied. While the break in slope in “ $(C_{11} - C_{12})$ ” occurs at the Néel point in zero field, it increases to ~ 12 K with 5 T in the $H\sigma$ configuration, and further to nearly 20 K, although more subtle, under 10 T. At 5 T in the H configuration, the transition is completely suppressed and no discernable change in slope takes place.

Meanwhile the “ C_{44} ” trace exhibits a much smaller effect upon the application of field and stress in a $H\sigma$ configuration, with almost complete suppression of the softening associated with T_N leading to a small stiffening (0.3 %) at 2 K. These effects do not remain when the field is taken off, suggesting that the response is more complicated than the analogous effect found by Petrović *et al.*¹¹, who reported that tetragonal domains could be permanently aligned by an electric field during cooling. The lack of change in f^2 at higher temperatures indicates that magnetic reorientation of the elastic microstructure has not taken place under our examined conditions.

Constant temperature, variable field/stress data also demonstrates significant changes from higher temperature regimes by 20 K, where, in a $H\sigma$ configuration, “ C_{44} ” stiffens after an initial softening, while “ $(C_{11} - C_{12})$ ” softens after an initial plateau. Below 5 K, the amplitude of the first point in the “ C_{44} ” data was uniformly too weak to be fitted, hence the absence of softening in the normalized data presented. A similar effect took place with applied field in the H measurement at 15 K and it is the first temperature at which changes appear to coincide with magnetic field alone, in this case giving a slight stiffening at higher fields. The most obvious observation is the existence of a number of low and high field/stress anomalies that are described in the results section and summarized on the tentative low temperature phase diagram below (with the hidden stress coordinate not calibrated).

The data near and below T_N are complementary to what was determined in our previous investigation³⁶. The further studies described here reveal a number of new trends that were unclear before, and we have also collected complementary information from the PC1 sample. We previously found evidence for elastic coupling to both the Néel transition and a lower temperature spin

reorientation transition³⁶. Evidence for both of these is also seen in magnetometry data, with the Néel point exhibiting a maximum and the spin reorientation displaying a distinct change in slope. This latter transition is not detected in some other studies⁹ when polycrystalline samples were used. Comparing the elastic behaviour near T_N without field between the SC and the PC1 sample reveals significant differences, including the disappearance of the anomaly at 2.6 K and the displacement down in temperature of the Q^{-1} peak associated with the Néel point in the SC sample. The softening near T_N in PC1 still correlates with T_N in our SC sample, at 5.6 K, while the peak in the loss is somewhat lower, shifted to ~ 4 K. The peak in Q^{-1} below T_N for the PC1 sample is significantly broader than observed in the SC sample, and may be related to defect concentration and distribution, in an analogous manner to the broadening of the C-T transition.

Compiling all of the information from the low temperature constant-temperature variable-field/stress measurements in the $H\sigma$ configuration and the new information on shifts in the softening associated with T_N under applied field, also in the $H\sigma$ configuration, along with those from our previous publication on ETO SC samples³⁶, we propose a tentative low temperature magnetic phase diagram including our measured anomalies, as well as the known lower-field transitions from Petrović *et al.*¹¹ (figure 26). Below the Néel point, we identified three additional, higher field/stress anomalies, with one anomaly between 1 T and 2 T, one between 5 T and 8 T and one between 11 T and 12 T, keeping in mind that the stress values increase with decreasing temperature. The lower and upper of these are from Ref.³⁶, while the in-between anomaly is identified here. The continuation of the high field anomaly to 10 K is clearly seen both in Ref.³⁶ and here, particularly for “ C_{44} ”. Finally, the anomaly seen at 1 T, 2 T and 3 T at 10 T, 15 T and 20 K respectively is reported in the present data and in Ref.³⁶. In addition to this $H\sigma$ data, H data are also shown on the figure as vertical bars indicating the windows of field in which significant changes in elastic properties were observed without applied stress. The position of these windows correlates quite closely with the points shown from the $H\sigma$ experiments, indicating that much of what was observed there was at least partially due to magnetism rather than to stress alone. The elasticity data do not, by themselves, indicate what magnetic or structural states might exist in the fields separated by the observed anomalies.

Possible explanations of the observed behaviour *Intrinsic character*

With respect to an explanation of the overall properties and behaviour of ETO in relation to intrinsic effects, a number of arguments were discussed in the introduction on the nature of octahedral tilting in ETO, the mechanism for magneto-electric and magneto-elastic coupling and phenomena such as coupling between the antiferrodistortive soft modes and magnetic field. The argu-

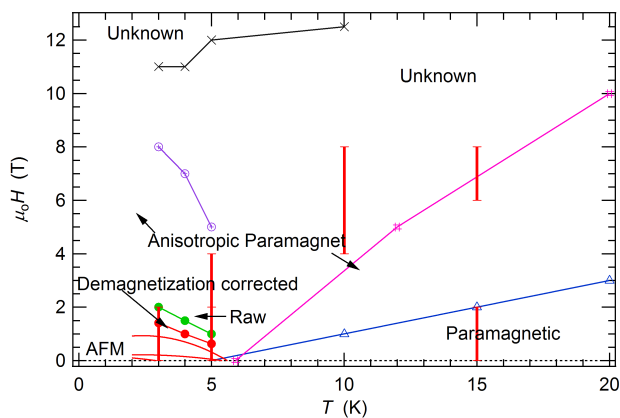


FIG. 26. A tentative low temperature phase diagram for ETO showing newly detected magnetic field/stress dependent anomalies and their relationship to known and unknown phases. Both raw and demagnetizing-factor corrected data are shown for the lowest field elastic anomaly. Markers with lines connecting them are from $H\sigma$ measurements, while the vertical bars indicate windows in which anomalies occurred for the H experiments.

ments of Birol and Fennie²⁰ in particular seem to suggest that driving the system into a ferromagnetic state will suppress the hybridization between Eu f electron shells and Ti d shells. This would allow the ferroelectric soft mode to become less stable, and as a result of competition between distortion modes will stabilize the antiferrodistortive soft mode. A more stable octahedral rotation soft mode promotes a decrease of the C-T transition temperature. The key message derived from the combination of measurements using both copper and steel transducer-rods is that stress triggers the softening associated with the phase transition, but that magnetic field alone has no measurable effect in our experiments.

As also discussed in the introduction, Rushchanskii *et al.*³¹ proposed that a number of antiferrodistorted structures are extremely close in energy. Both they and Yang *et al.*³⁴ suggest that a “phase coexistence” in real samples may be possible due to small energy differences. This allows the formation of incommensurate phases or local changes in tilt ordering under small energy perturbations. Rushchanskii *et al.*³¹ also detailed spin-phonon coupling, with induced ferromagnetism hardening the octahedral tilting phonon mode significantly (and thus lowering the transition temperature), 50 cm^{-1} , in I4/mcm, but softening slightly (and thereby increasing the transition temperature), 17 cm^{-1} , in $R\bar{3}c$. Coexisting “tilted phases” lead to an arrangement with octahedral tilt disorder due to a short correlation length perpendicular to the plane of octahedral rotation. The disordered, locally tetragonal, but cubic on average arrangement found by Alietta *et al.*¹⁰ may be created in this way, as well as intermediate results such as the incommensurate ordering observed by Goain *et al.*⁹ and Kim *et al.*¹². This arrange-

ment also admits an explanation of the high loss in both “ $(C_{11} - C_{12})$ ” and “ (C_{44}) ”, as local rhombohedral distortions are expected, and defects associated with areas of these types will indeed be susceptible to stresses associated with “ (C_{44}) ”, but which would not be found in a fully ordered I4/mcm phase. The local rhombohedral disorder never extends to form a long range ordered state with decreasing temperature, while the tetragonal order locks in.

It is known that incommensurate systems (particularly those with incommensurate structural screw-axes of the type shown in figure 1c of Ref. 12) may take hours or even days to reach equilibrium after changes in temperature⁴¹, admitting seemingly equivalent final states to be non-equilibrium on the timescale of the measurements described here, for example the shift in temperature of the loss peak associated with T_S under poling or the hysteresis and time dependence in constant temperature-variable field mode, both $H\sigma$ and H , between 215 K and T_S .

Extrinsic character

We have argued that the anelastic behaviour of ETO could be understood in terms of a significant role for defects which are mobile on a time scale of $\sim 10^{-6}$ s and temperatures above $\sim (150 \text{ to } 200)$ K, even though direct evidence is not available. The concentration of defects that are present in different samples of ETO can vary significantly, as discussed by Goain *et al.*⁹, and in addition, grain boundaries provide heterogeneous sites that act as pinning centers for local ordering.

The changes in elastic and anelastic properties observed with applied field and stress are evidently not exclusively related to a bulk magnetic order in ETO, as the phenomena extend to far above the magnetic ordering temperatures. It is possible that some contribution to this behaviour stems from magnetism in the domain walls. Domain walls which involve changes in two order parameters simultaneously develop local structures which are distinct from those of the adjacent homogeneous domains. This enables the development of ferroelectricity in the domain walls of nonferroelectric STO^{39,42}, for example. In this scenario, a gradient of the order parameter exists in the walls, and gradient-gradient coupling between order parameters or with strain, can occur^{43–45}. Lateral movement of domain walls in ferroelastics, more generally, can take place by movement of ledges along the walls^{46,47}. The relatively low acoustic loss observed in ETO, in comparison with STO, and the lack of Debye freezing behaviour, has been considered here to be indicative of relatively immobile twin walls and the pinning mechanism could be related to local relaxations of the ledges. The influence of magnetism in the domain walls is in accordance with transport results of Bussmann-Holder *et al.* (unpublished), which can be explained by large in-wall magnetostriction.

From an atomic point of view, pinning centres are likely to originate either from defects associated with Eu, for example vacancies, local changes in valence, or from

oxygen vacancies. In this context it is interesting to note the recent work of Lopez-Bezanilla et al.³³ that valence flexibility in Ti ions, coupled with oxygen vacancies, can produce magnetic defect clusters in STO.

V. CONCLUSIONS

This study, using RUS with applied magnetic field, has enabled us to highlight the role of magnetoelastic coupling in the behaviour of ETO. The key results of this examination are as follows:

(i) Defects play a key role in the elastic and anelastic behaviour.

(ii) Pinning of the ferroelastic twin walls appears to occur immediately below the cubic-tetragonal transition.

(iii) The influence of defects rather than only ferroelastic twin walls *per se* is clear as the stress influence on elastic resonances associated with both tetragonal and rhombohedral strain (“ $C_{11} - C_{12}$ ” and “ C_{44} ” respectively) in constant field-variable temperature measurements are similar, despite only “ $C_{11} - C_{12}$ ” being related to relaxation of the microstructure. Furthermore, the influence of poling on these defects persists into the cubic phase, where microstructure should not play a role.

(iv) Metastability was found to occur, with relaxations of elastic constants at constant field/stress with variable temperature leading to hysteresis/time relaxation from ~ 200 K to $T_S = 282$ K. This effect is stronger in “ $C_{11} - C_{12}$ ” than “ C_{44} ”, suggesting some involvement of microstructure.

(v) This metastability was further demonstrated by contrasting effects near T_S with applied magnetic field and stress in constant field-variable temperature and constant temperature-variable field/stress measurements, with the former lowering the elastic anomaly by ~ 0.4 K and the latter appearing to drive the phase transition, thus having the opposite effect on the elastic properties. The application of magnetic field alone was found to have no apparent effect on T_S and thus the main driver for

these changes must be the applied stress in the $H\sigma$ configuration.

(vi) Differences between the examined single crystal sample and two differently prepared polycrystalline samples most likely stem from defect types and concentrations and have implications for conflicting results in the literature.

(vii) Magnetic/stress poling at low temperatures was found to raise the temperature of the main elastic anomaly at T_S by ~ 2 K and to slightly alter the frequency of the measured “ $C_{11} - C_{12}$ ”-like peak, emphasising its influence on microstructure. Later measurements on the sample in H configuration, even without field, yielded still higher transition temperatures, suggesting that the memory effect of the poling regime lasts at least on the time scale of months, as the interval between these measurements was of the order of more than 10 months.

(viii) A number of anomalies below 50 K were related to known magnetic transitions and to unknown effects, allowing the tentative construction of a low-temperature phase diagram.

VI. ACKNOWLEDGMENTS

MAC acknowledges support from NERC and EPSRC (grants NE/B505738/1 and EP/I036079/1, respectively). CP acknowledges financial support in Greece through FP7-REGPOT-2012-2013-1, and in Singapore through Award No. NRF-CRP-4-2008-04 of the Competitive Research Programme. LJS acknowledges the support of the National Science Centre (NCN) through grant MAESTRO no. DEC-2012/04/A/ST3/00342. Dr Albert Migliori (Los Alamos National Laboratory) is thanked for invaluable assistance in creating the RUS system with in-situ magnetic field. Prof Jim Scott (U. Cambridge) is thanked for his advice and assistance in interpreting the data and improving the manuscript. Tony Dennis (U. Cambridge) collected the SQUID data.

* email:mc43@cam.ac.uk

¹ T. R. McGuire, M. W. Shafer, R. J. Joenk, H. A. Alperin, and S. J. Pickart, *Journal of Applied Physics* **37**, 981 (1966), URL <http://scitation.aip.org/content/aip/journal/jap/37/3/10.1063/1.1708549>.

² T. Katsufuji and H. Takagi, *Phys. Rev. B* **64**, 054415 (2001), URL <http://link.aps.org/doi/10.1103/PhysRevB.64.054415>.

³ T. Katsufuji and Y. Tokura, *Phys. Rev. B* **60**, R15021 (1999), URL <http://link.aps.org/doi/10.1103/PhysRevB.60.R15021>.

⁴ A. Bussmann-Holder, Z. Guguchia, J. Köhler, H. Keller, a. Shengelaya, and a. R. Bishop, *New Journal of Physics* **14**, 093013 (2012), ISSN 1367-2630, URL <http://stacks.iop.org/1367-2630/14/i=9/a=093013?key=crossref.36e8a9b5484e0ad44ce900edced9bfb0>.

⁵ A. Bussmann-Holder, J. Köhler, R. K. Kremer, and J. M. Law, *Phys. Rev. B* **83**, 212102 (2011), URL <http://link.aps.org/doi/10.1103/PhysRevB.83.212102>.

⁶ J. L. Bettis, M.-H. Whangbo, J. Köhler, A. Bussmann-Holder, and a. R. Bishop, *Physical Review B* **84**, 184114 (2011), ISSN 1098-0121, URL <http://link.aps.org/doi/10.1103/PhysRevB.84.184114>.

⁷ D. S. Ellis, H. Uchiyama, S. Tsutsui, K. Sugimoto, K. Kato, D. Ishikawa, and A. Q. R. Baron, *Phys. Rev. B* **86**, 220301 (2012), URL <http://link.aps.org/doi/10.1103/PhysRevB.86.220301>.

⁸ S. Kamba, D. Nuzhnyy, P. Vaněk, M. Savinov, K. Knížek, Z. Shen, E. Šantavá, K. Maca, M. Sadowski, and J. Petzelt, *Europhysics Letters (EPL)* **80**, 27002 (2007), ISSN 0295-5075, URL <http://stacks.iop.org/0295-5075/80/i=2/a=27002>

- key=crossref.d33918e7563eb3ba4983c1b1f287850e.
- ⁹ V. Goian, S. Kamba, O. Pacherová, J. Dražokoupil, L. Palatinus, M. Dušek, J. Rohlíček, M. Savinov, F. Laufek, W. Schranz, et al., *Phys. Rev. B* **86**, 054112 (2012), URL <http://link.aps.org/doi/10.1103/PhysRevB.86.054112>.
 - ¹⁰ M. Allieta, M. Scavini, L. J. Spalek, V. Scagnoli, H. C. Walker, C. Panagopoulos, S. S. Saxena, T. Katsufuji, and C. Mazzoli, *Phys. Rev. B* **85**, 184107 (2012), URL <http://link.aps.org/doi/10.1103/PhysRevB.85.184107>.
 - ¹¹ A. P. Petrovic, Y. Kato, S. S. Sunku, T. Ito, P. Sengupta, L. Spalek, M. Shimuta, T. Katsufuji, C. D. Batista, S. S. Saxena, et al., *Phys. Rev. B* **87**, 064103 (2013), URL <http://link.aps.org/doi/10.1103/PhysRevB.87.064103>.
 - ¹² J.-W. Kim, P. Thompson, S. Brown, P. S. Normile, J. A. Schlueter, A. Shkabko, A. Weidenkaff, and P. J. Ryan, *Phys. Rev. Lett.* **110**, 027201 (2013), URL <http://link.aps.org/doi/10.1103/PhysRevLett.110.027201>.
 - ¹³ D. Bessas, K. Z. Rushchanskii, M. Kachlik, S. Disch, O. Gourdon, J. Bednarcik, K. Maca, I. Sergueev, S. Kamba, M. Ležaić, et al., *Physical Review B* **88**, 144308 (2013), ISSN 1098-0121, URL <http://link.aps.org/doi/10.1103/PhysRevB.88.144308>.
 - ¹⁴ K. Caslin, R. K. Kremer, Z. Guguchia, H. Keller, J. Köhler, and A. Bussmann-Holder, *Journal of physics. Condensed matter : an Institute of Physics journal* **26**, 022202 (2014), ISSN 1361-648X, URL <http://www.ncbi.nlm.nih.gov/pubmed/24275498>.
 - ¹⁵ V. Scagnoli, M. Allieta, H. Walker, M. Scavini, T. Katsufuji, L. Sagarna, O. Zaharko, and C. Mazzoli, *Physical Review B* **86**, 094432 (2012), ISSN 1098-0121, URL <http://link.aps.org/doi/10.1103/PhysRevB.86.094432>.
 - ¹⁶ V. Goian, S. Kamba, J. Hlinka, P. Vaněk, a. a. Belik, T. Kolodiazhnyi, and J. Petzelt, *The European Physical Journal B* **71**, 429 (2009), ISSN 1434-6028, URL <http://www.springerlink.com/index/10.1140/epjb/e2009-00205-5>.
 - ¹⁷ J. Köhler, R. Dinnebier, and A. Bussmann-Holder, *Phase Transitions* **85**, 949 (2012), <http://dx.doi.org/10.1080/01411594.2012.709634>, URL <http://dx.doi.org/10.1080/01411594.2012.709634>.
 - ¹⁸ L. J. Spalek, Ph.D. thesis, University of Cambridge (2013).
 - ¹⁹ Q. Jiang and H. Wu, *Journal of Applied Physics* **93**, 2121 (2003), URL <http://scitation.aip.org/content/aip/journal/jap/93/4/10.1063/1.1540226>.
 - ²⁰ T. Birol and C. J. Fennie, *Physical Review B* **88**, 094103 (2013), ISSN 1098-0121, URL <http://link.aps.org/doi/10.1103/PhysRevB.88.094103>.
 - ²¹ K. A. Müller and H. Burkard, *Phys. Rev. B* **19**, 3593 (1979), URL <http://link.aps.org/doi/10.1103/PhysRevB.19.3593>.
 - ²² H. Akamatsu, Y. Kumagai, F. Oba, K. Fujita, H. Murakami, K. Tanaka, and I. Tanaka, *Physical Review B* **83**, 214421 (2011), ISSN 1098-0121, URL <http://link.aps.org/doi/10.1103/PhysRevB.83.214421>.
 - ²³ P. J. Ryan, J.-W. Kim, T. Birol, P. Thompson, J.-H. Lee, X. Ke, P. S. Normile, E. Karapetrova, P. Schiffer, S. D. Brown, et al., *Nature communications* **4**, 1334 (2013), ISSN 2041-1723, URL <http://www.ncbi.nlm.nih.gov/pubmed/23299884>.
 - ²⁴ M. D. Glinchuk, E. a. Eliseev, Y. Gu, L.-Q. Chen, V. Gopalan, and A. N. Morozovska, *Physical Review B* **89**, 014112 (2014), ISSN 1098-0121, URL <http://link.aps.org/doi/10.1103/PhysRevB.89.014112>.
 - ²⁵ W. Li, R. Zhao, L. Wang, R. Tang, Y. Zhu, J. H. Lee, H. Cao, T. Cai, H. Guo, C. Wang, et al., *Scientific reports* **3**, 2618 (2013), ISSN 2045-2322, URL <http://www.pubmedcentral.nih.gov/articlerender.fcgi?artid=3767944&tool=pmcentrez&rendertype=abstract>.
 - ²⁶ C. J. Fennie and K. M. Rabe, *Phys. Rev. Lett.* **97**, 267602 (2006), URL <http://link.aps.org/doi/10.1103/PhysRevLett.97.267602>.
 - ²⁷ R. Ranjan, H. S. Nabi, and R. Pentcheva, *Journal of Physics: Condensed Matter* **19**, 406217 (2007), URL <http://stacks.iop.org/0953-8984/19/i=40/a=406217>.
 - ²⁸ J. H. Lee, L. Fang, E. Vlahos, X. Ke, Y. W. Jung, L. F. Kourkoutis, J.-W. Kim, P. J. Ryan, T. Heeg, M. Roeckerath, et al., *Nature* **466**, 954 (2010), ISSN 0028-0836, URL <http://dx.doi.org/10.1038/nature09331>.
 - ²⁹ A. N. Morozovska, M. D. Glinchuk, R. K. Behera, B. Zalyuchny, C. S. Deo, and E. a. Eliseev, *Physical Review B* **84**, 205403 (2011), ISSN 1098-0121, URL <http://link.aps.org/doi/10.1103/PhysRevB.84.205403>.
 - ³⁰ Y. Geng, J. Lee, D. Schlom, J. Freeland, and W. Wu, *Physical Review B* **87**, 121109 (2013), ISSN 1098-0121, URL <http://link.aps.org/doi/10.1103/PhysRevB.87.121109>.
 - ³¹ K. Z. Rushchanskii, N. a. Spaldin, and M. Ležaić, *Physical Review B* **85**, 104109 (2012), ISSN 1098-0121, URL <http://link.aps.org/doi/10.1103/PhysRevB.85.104109>.
 - ³² D. S. Ellis, H. Uchiyama, S. Tsutsui, K. Sugimoto, K. Kato, and A. Q. Baron, *Physica B: Condensed Matter* **442**, 34 (2014), ISSN 09214526, URL <http://linkinghub.elsevier.com/retrieve/pii/S0921452614001288>.
 - ³³ A. Lopez-Bezanilla, P. Ganesh, and P. B. Littlewood, arXiv pp. 1–6 (2015), arXiv:1502.05749v1.
 - ³⁴ Y. Yang, W. Ren, D. Wang, and L. Bellaiche, *Phys. Rev. Lett.* **109**, 267602 (2012), URL <http://link.aps.org/doi/10.1103/PhysRevLett.109.267602>.
 - ³⁵ L. J. Spalek, S. S. Saxena, C. Panagopoulos, T. Katsufuji, J. A. Schiemer, and M. A. Carpenter, *Phys. Rev. B* **90**, 054119 (2014).
 - ³⁶ J. Schiemer, L. J. Spalek, S. S. Saxena, C. Panagopoulos, T. Katsufuji, and M. A. Carpenter, *Europhysics Letters* **109**, 57004 (2015), URL <http://dx.doi.org/10.1209/0295-5075/109/57004>.
 - ³⁷ Z. Guguchia, H. Keller, J. Köhler, and A. Bussmann-Holder, *Journal of Physics: Condensed Matter* **24**, 492201 (2012), URL <http://stacks.iop.org/0953-8984/24/i=49/a=492201>.
 - ³⁸ R. E. McKnight, M. A. Carpenter, T. W. Darling, A. Buckley, and P. A. Taylor, *Am. Mineral.* **92**, 1665 (2007), URL <http://ammin.geoscienceworld.org/content/92/10/1665.abstract>.
 - ³⁹ J. F. Scott, E. K. H. Salje, and M. A. Carpenter, *Phys. Rev. Lett.* **109**, 187601 (2012), URL <http://link.aps.org/doi/10.1103/PhysRevLett.109.187601>.
 - ⁴⁰ B. J. Kennedy, G. Murphy, E. Reynolds, M. Avdeev, H. E. R. Brand, and T. Kolodiazhnyi, *Journal of Physics: Condensed Matter* **26**, 495901 (2014), URL <http://stacks.iop.org/0953-8984/26/i=49/a=495901>.
 - ⁴¹ J. F. Scott, *Journal of physics. Condensed matter : an Institute of Physics journal* **25**, 331001 (2013), ISSN 1361-648X, URL [http://iopscience.iop.org/0953-8984/25/33/331001/\\$\backslashbackslashbackslashnhttp://www.ncbi.nlm.nih.gov/pubmed/23877925](http://iopscience.iop.org/0953-8984/25/33/331001/$\backslashbackslashbackslashnhttp://www.ncbi.nlm.nih.gov/pubmed/23877925).
 - ⁴² T. Zykova-Timan and E. K. H. Salje, *Applied Physics Letters* **104**, 082907 (2014), URL

<http://scitation.aip.org/content/aip/journal/apl/104/8/10.1063/1.4866859>.

- ⁴³ B. Houchmanzadeh, J. Lajzerowicz, and E. Salje, *Phase Transitions* **38**, 77 (1992), ISSN 0141-1594, URL <http://www.tandfonline.com/doi/abs/10.1080/01411599208203464>.
- ⁴⁴ E. a. Eliseev, S. V. Kalinin, Y. Gu, M. D. Glinchuk, V. Khist, A. Borisevich, V. Gopalan, L. Q. Chen, and A. N. Morozovska, *Physical Review B - Condensed Matter and Materials Physics* **88**, 1 (2013), ISSN 10980121, 1301.2360.
- ⁴⁵ P. V. Yudin, a. K. Tagantsev, and N. Setter, *Physical Review B - Condensed Matter and Materials Physics* **88**, 1 (2013), ISSN 10980121.
- ⁴⁶ M. A. Carpenter and Z. Zhang, *Geophysical Journal International* **186**, 279 (2011), <http://gji.oxfordjournals.org/content/186/1/279.full.pdf+html>, URL <http://gji.oxfordjournals.org/content/186/1/279.abstract>.
- ⁴⁷ E. K. H. Salje, X. Ding, Z. Zhao, T. Lookman, and A. Saxena, *Phys. Rev. B* **83**, 104109 (2011), URL <http://link.aps.org/doi/10.1103/PhysRevB.83.104109>.